Biomaterials Advances 151 (2023) 213429

Contents lists available at ScienceDirect

Biomaterials Advances

journal homepage: www.journals.elsevier.com/materials-science-and-engineering-c

It takes two to remyelinate: A bioengineered platform to study astrocyte-oligodendrocyte crosstalk and potential therapeutic targets in remyelination

Daniela N. Rocha [a,b,c,1], Eva D. Carvalho [a,b,c,1], Liliana R. Pires [b,c], Chiara Gardin [d], Ilaria Zanolla [e], Piotr K. Szewczyk [f], Cláudia Machado [a], Rui Fernandes [a], Urszula Stachewicz [f], Barbara Zavan [e], João B. Relvas [a,g,h], Ana P. Pêgo [a,b,i,*]

[a] Instituto de Investigação e Inovação em Saúde (i3S), Universidade do Porto, 4200-135 Porto, Portugal
[b] Instituto de Engenharia Biomédica (INEB), Universidade do Porto, 4200-135 Porto, Portugal
[c] Faculdade de Engenharia da Universidade do Porto (FEUP), 4200-465 Porto, Portugal
[d] Maria Cecilia Hospital, GVM Care & Research, Cotignola, 48033 Ravenna, Italy
[e] Department of Translational Medicine, University of Ferrara, 44121 Ferrara, Italy
[f] Faculty of Metals Engineering and Industrial Computer Science, AGH University of Science and Technology, 30-059 Krakow, Poland
[g] Instituto de Biologia Molecular e Celular (IBMC), Universidade do Porto, 4200-135 Porto, Portugal
[h] Department of Biomedicine, Faculty of Medicine, Universidade do Porto, 4200-319 Porto, Portugal
[i] Instituto de Ciências Biomédicas Abel Salazar (ICBAS), Universidade do Porto, 4050-343 Porto, Portugal

ARTICLE INFO

Keywords:
Polymer microfibres
Oligodendrocyte
Myelination
Alginate hydrogel
Astrogliosis
RhoA

ABSTRACT

The loss of the myelin sheath insulating axons is the hallmark of demyelinating diseases. These pathologies often lead to irreversible neurological impairment and patient disability. No effective therapies are currently available to promote remyelination.

Several elements contribute to the inadequacy of remyelination, thus understanding the intricacies of the cellular and signaling microenvironment of the remyelination niche might help us to devise better strategies to enhance remyelination.

Here, using a new *in vitro* rapid myelinating artificial axon system based on engineered microfibres, we investigated how reactive astrocytes influence oligodendrocyte (OL) differentiation and myelination ability. This artificial axon culture system enables the effective uncoupling of molecular cues from the biophysical properties of the axons, allowing the detailed study of the astrocyte-OL crosstalk. Oligodendrocyte precursor cells (OPCs) were cultured on poly(trimethylene carbonate-*co*-ε-caprolactone) copolymer electrospun microfibres that served as surrogate axons. This platform was then combined with a previously established tissue engineered glial scar model of astrocytes embedded in 1 % (*w/v*) alginate matrices, in which astrocyte reactive phenotype was acquired using meningeal fibroblast conditioned medium.

OPCs were shown to adhere to uncoated engineered microfibres and differentiate into myelinating OL. Reactive astrocytes were found to significantly impair OL differentiation ability, after six and eight days in a co-culture system. Differentiation impairment was seen to be correlated with astrocytic miRNA release through exosomes. We found significantly reduction on the expression of pro-myelinating miRNAs (miR-219 and miR-338) and an increase in anti-myelinating miRNA (miR-125a-3p) content between reactive and quiescent astrocytes. Additionally, we show that OPC differentiation inhibition could be reverted by rescuing the activated astrocytic phenotype with ibuprofen, a chemical inhibitor of the small rhoGTPase RhoA.

Overall, these findings show that modulating astrocytic function might be an interesting therapeutic avenue for demyelinating diseases. The use of these engineered microfibres as an artificial axon culture system will enable the screening for potential therapeutic agents that promote OL differentiation and myelination while providing valuable insight on the myelination/remyelination processes.

* Corresponding author at: Instituto de Investigação e Inovação em Saúde (i3S), Universidade do Porto, 4200-135 Porto, Portugal.
E-mail address: apego@i3s.up.pt (A.P. Pêgo).
[1] Equal contribution.

https://doi.org/10.1016/j.bioadv.2023.213429
Received 15 August 2022; Received in revised form 21 March 2023; Accepted 12 April 2023
Available online 25 April 2023
2772-9508/© 2023 The Authors. Published by Elsevier B.V. This is an open access article under the CC BY-NC-ND license (http://creativecommons.org/licenses/by-nc-nd/4.0/).

1. Introduction

Demyelinating diseases of the central nervous system (CNS) represent one of the main debilitating neurological conditions affecting patients at various stages of life, being the most frequently occurring one multiple sclerosis (MS) [1]. These diseases are characterized by the loss of myelin – a dielectric membrane produced by oligodendrocytes (OLs) that insulates axons. Often, myelin loss can be partially rescued by remyelination of spared axons, nonetheless this phenomenon is limited to the early onset of diseases and is variable among patients [2]. In time, remyelination failure leads to axonal degeneration and, eventually neuronal death, with irreversible patient functional failure. Understanding why remyelination fails in demyelinating conditions is a critical need for the design of therapeutical approaches against these diseases.

Although an extensive debate on the origin of the remyelinating OLs exists, evidence show that myelin repair can be achieved by oligodendrocyte precursor cells (OPCs) or mature OLs surviving an episode of demyelination [2,3]. Failure of remyelination has been attributed to the microenvironment of the chronic demyelinating lesion, which is not conducive to OPC differentiation and maturation.

Many OL differentiation inhibitory molecules and putative related signaling pathways have been described. However, so far the proposed therapies have proven inefficient due to the complexity of the disease [4]. Recent findings point towards a crucial role of the extracellular matrix (ECM) on modulating the OPC/OL differentiation processes [5]. Extensive matrix remodelling has been shown in animal models of demyelination as well as in human brains [6,7]. This remodulation can affect the biophysical properties of the tissue [8]. For instance, demyelination causes softening of the tissues while remyelination increases the stiffness of the same areas in human MS lesions. Similar changes in the mechanical properties of the brain were also observed in a mouse model of demyelination. Interestingly, chronic demyelination was associated with increase stiffening of the tissue [9].

Astrocytes are thought to play a central role in the remodelling of brain ECM. These cells communicate with OLs during development and homeostasis so that myelination can occur in an accurate and timely manner [10–12]. In demyelinating conditions, aberrant astrocytic activation has been linked to disease progression, as secreted proteins can be found in cerebrospinal fluid (CSF) samples of patients (for instance, matrix metalloproteinase-7 (MMP-7) and SERPINA3) [13–15]. Astrogliosis occurs when astrocytes become activated expressing high levels of glial fibrillary acidic protein (GFAP) and vimentin. These cells also secrete considerable amounts of ECM components such as chondroitin sulfate proteoglycans (CSPG) and collagen IV and, at a chronic phase of the disease, are responsible for forming a glial scar [15]. In fact, acute demyelinating lesions were proved to evolve to chronic active lesions with an astroglial scar in the centre surrounded by inflammatory cells at the lesion rim [16]. The glial scar, which initially limits the inflammation of the lesioned tissue, gradually becomes a biochemical and mechanical obstacle to remyelination [17].

We have previously reported an alginate-based 3D model of astrogliosis [18] where astrocytes cultured in the presence of meningeal fibroblast conditioned medium (CM) behave similarly to glial scar astrocytes, showing changes in gene expression (*e.g.*, GFAP), increased ECM production (chondroitin 4-sulfate and collagen type IV) and inhibiting neuronal outgrowth. This behaviour was found to be influenced by the hydrogel network mechanical properties, with astrocyte activation being mediated *via* the Ras homolog family member A (RhoA), a small GTPase involved in mechanosensing pathways. The pharmacological inhibition of RhoA rescued the astrocyte phenotype.

Here, we hypothesize that OPC differentiation is hindered by astrocyte reactivity and that cell-cell communication vesicles (exosomes) play an important role in this inhibition. Furthermore, we postulate that the reversion of the astrocyte phenotype to a non-activated status can lead to the recovery of the OL differentiation capacity.

To test this hypothesis we used an *in vitro* rapid myelinating artificial axon system composed by electrospun poly(trimethylene-*co*-ε-caprolactone) (P(TMC-CL)) fibres combined with a tissue engineered glial scar as a tool to dissect the crosstalk between reactive astrocytes and OLs. Previous studies have demonstrated the reliability of using polymeric electrospun fibres for mimicking axons and promote OL myelination [19–21]. P(TMC-CL) is a *co*-polymer of poly(caprolactone) and poly (trimethyl carbonate) which was previously proved to be a suitable substrate for growing neural cells, including Schwann cells [22,23] and for nerve conduit preparation promoting peripheral nerve regeneration [24,25]. Furthermore, electrospun fibres from P(TMC-CL) polymer can be easily and rapidly obtained [26]. The use of engineered polymeric microfibres to serve as axon mimetics enabled the singled study of the astrocyte-OL crosstalk and its influence on OL differentiation ability in a relevant way.

2. Materials and methods

2.1. Poly(trimethylene carbonate-co-ε-caprolactone) (P(TMC-CL)) fibre preparation and characterization

P(TMC-CL) was synthesized as previously described [24]. Briefly, prior to polymerization ε-caprolactone monomer (Fluka) was dried overnight over CaH_2 and distilled under reduced pressure. Trimethylene carbonate was obtained from Boehringer Ingelheim (Germany) and used as received. Polymerizations were conducted by ring-opening polymerization in an argon atmosphere using stannous octoate as a catalyst (proportion of 2×10^{-4} mol per mol of monomer). All polymerizations were carried out for a period of 3 days in an oil bath pre-heated to 130 °C. The obtained polymers were purified by dissolution in chloroform (3 % (*w/v*)) and subsequent precipitation into a ten-fold volume of ethanol. The precipitated polymers were recovered, washed with fresh ethanol, and dried under reduced pressure at room temperature (RT) until constant weight. The prepared polymers were characterized with respect to chemical composition by ^{1}H nuclear magnetic resonance (NMR) and found to contain 11 % mol of TMC, which was in accordance with the monomer ratio charged (10 % mol TMC). The number average number molecular weight and polydispersity index of the purified polymer were determined by size exclusion chromatography using chloroform as the mobile phase and conventional calibration (see Supplementary Table 1).

P(TMC-CL) fibres were obtained by electrospinning using a polymer solution (10 % *w/v*) in a dichloromethane:dimethylformamide 3:1 or 6:1 mixture (DCM:DMF; Merck, Germany) as reported elsewhere [27]. The polymer solution was dispensed at a controlled flow rate of 0.9–1.0 mL/h using a syringe pump (Ugo Basile, Italy). An electric field between 14 and 16 kV was applied (Gamma High Voltage Research, Inc., FL, USA) between the spinneret (outer diameter 0.8 mm) and the flat collector (Aluminium foil, 15 × 15 cm), distanced 14–16 cm. Fibres were collected during 1–1.5 h onto 13 mm glass coverslips (Menzel-Glaser, Germany) distributed on top of aluminium foil. Temperature and humidity were always registered (average values of 25 °C and 40 % RH).

Fibre morphology was analysed by scanning electron microscopy (SEM). A JEOL JSM 6301F/Oxford INCA Energy 350/Gatan Alto 2500 was used. Fibre diameter was quantified from SEM micrographs using image analysis software Image J (version 1.39; NIH, Bethesda, MD, USA). Prior analysis, samples were coated with an Au/Pd thin film for 70 s and with a 15 mA current, by sputtering, using the SPI Module Sputter Coater equipment. Fibre-mean diameter and fibre distribution were calculated from at least 100 measurements from four different electrospinning fabrication batches using image analysis software (ImageJ, version 1.50b; Rasband, W.S., ImageJ, U. S. National Institutes of Health, Maryland, USA) [28].

2.2. Cell cultures

All procedures involving animals and their care were performed in agreement with institutional ethical guidelines (IBMC/INEB/i3S), the EU directive (2010/63/EU) and Portuguese law (DL 113/2013). Experiments described here had the approval of Portuguese Veterinary Authorities. Animals had free access to food and water, being kept under a 12-h light/12-h dark cycle.

Primary cultures of OPCs and astrocytes were obtained as previously described [29,30]. Briefly, mixed glial cultures were isolated from the brains of post-natal day 0 to day 2 (P0-P2) Wistar Han rats. Pups were sacrificed by decapitation and brain removed from and collected in a Petri dish containing Hank's Balanced Salt Solution without calcium and magnesium (HBSS, Sigma) supplemented with 2 % (*v*/v) penicillin/streptavidin (P/S) and maintained on ice (to decrease tissue degradation and cell death). Brain hemispheres were separated with thin forceps, and the meningeal tissue, the cerebellum, the basal ganglia and the hippocampus were removed. The isolated frontal cortices were maintained in HBSS 2 % (*v*/v) P/S and on ice until dissociation. Isolated cortices were digested in HBSS without calcium or magnesium supplemented with trypsin (0.0025 % (*w/v*)) and 0.001 mg/mL DNAse I (Applichem Life-Sciences) for 15 min at 37 °C. Dissociated cortices were cultured in 100 μg/mL poly(L-lysine) (PLL, diluted in deionized water, Sigma-Aldrich) coated 75 cm^2 flasks (30 min, 37 °C and 5 % CO_2) and maintained in Dulbecco's Modified Eagle Medium (DMEM) supplemented with 10 % (*v*/v) heat-inactivated (30 min, 56 °C) foetal bovine serum (FBS) and 1 % (v/v) P/S, hereafter designed DMEM medium. Cells were grown in a cell culture incubator at 37 °C and 5 % CO_2. When confluence was reached (~12 days) the flasks were submitted to a pre-shake (210 rpm, 2 h, 37 °C) causing detachment of microglia. Medium with detached microglia was removed and culture medium was refreshed. Following a 2 h incubation period (37 °C, 5 % CO_2), MGCs were submitted to shake-off (230 rpm, overnight, 37 °C), resulting in detachment of OPCs and remaining microglia (while astrocytes remain adhered during this procedure). Medium with detached OPCs and microglia was transferred to non-coated and non-treated Petri dishes (90 mm, Normax) and incubated for 2 h (37 °C, 5 % CO_2). Microglia adheres faster to non-treated substrates than OPCs, allowing for the removal of the remaining microglia. Medium with OPCs in suspension was collected from the Petri dishes and transferred to a Falcon tube through a 40 μm nylon cell strainer (Falcon) to remove astrocyte clusters that could possibly have detached during shaking.

OPCs were then seeded on the top of polymeric fibres or PLL pre-coated glass coverslips (50 μg/mL, 30 min, 37 °C and 5 % CO_2,) and maintained for 24 h in OPC SATO medium which was composed by DMEM medium supplemented with apo-transferrin (0.1 mg/mL, Merck T2036), bovine serum albumin (BSA) (0.1 mg/mL, NZYTech MB04601), putrescin (16 μg/mL, Sigma P7505), progesterone (60 ng/mL, Sigma P8783-), thyroxine (40 ng/mL, Merck T1775), sodium selenite (40 ng/mL, Sigma 214485-), triiodo-L-thyroxine (30 ng/mL, Merck T1775), insulin (5 μg/mL, Sigma I9278), recombinant human platelet derived growth factor-AA (PDGF-AA) (0.01 μg/mL, Peprotech 100-13A), recombinant human fibroblast growth factor (FGF) (0.01 μg/mL, Peprotech 100-18B) and 1 % (*v*/v) P/S. After 24 h of culture in the presence of OPC SATO, cell differentiation was induced. Medium was replaced by OL SATO, which has the same components of the OPC SATO with exception of PDGF-AA and FGF. These components were removed and 0.5 % heat-inactivated (30 min, 56 °C) FBS was added to the medium.

The purity of each culture was estimated by immunocytochemistry over 2, 4 and 8 days *in vitro* (DIV). Please refer to the section "2.4 Immunocytochemistry" for further details on the immunocytochemistry procedure. Only cultures with more than around 80 % of purity were used in further studies. Microglia (maximum 10 %), and a small percentage of astrocytes (maximum 4 %) were present in the cultures, which is in accordance with previous reports (Supplementary Fig. S1). The remaining cells adhered to the 75 cm^2 flasks after shaking were mainly astrocytes, which were trypsinized and re-cultured in new flasks in DMEM medium. Further tripsinizations were performed to increase culture purity [30–32]. Cells were used from passage 3 to passage 5. The final astrocyte culture purity was estimated >90 % (data not shown). Microglia (maximum 7 %), and a small percentage of OPCs and neurons (maximum 1 %) were present in the cultures but did not influence the normal behaviour of astrocytes (data not shown).

Meningeal fibroblasts were obtained from brain meninges of P0-P2 Wistar Han rats. Upon isolation, meningeal tissue was digested in HBSS without calcium or magnesium and supplemented with trypsin (0.0025 % (*w/v*)) and 0.001 mg/mL DNAse for 30 min. Dissociated meninges were plated in PLL coated 75 cm^2 flasks (100 μg/mL, diluted in deionized water, 30 min, 37 °C 5 % CO_2) and maintained in DMEM medium. Meningeal fibroblast conditioned medium (CM) was obtained by culturing 1.33×10^3 cells/cm^2 in DMEM medium for 72 h. After collection, CM was centrifuged (500*g*, 10 min) and stored at 4 °C until use (maximum storage time one week).

Of note, an independent experiment was considered for OPCs derived from different MGC shake off and/or astrocytes from different passages.

2.3. Tissue engineered glial scar

In situ forming alginate hydrogel matrices were prepared as previously described [18,33]. Briefly, PRONOVA ultrapure sodium alginates LVG and VLVG (hereafter designated as high and low molecular weight, HMW and LMW, respectively) with a high guluronic acid content (68 %) were purchased from FMC Biopolymers. Hydrogel-precursor solutions with a bimodal molecular weight composition were prepared by combining 1 % (*w/v*) HMW and LMW alginate solution in 0.9 % NaCl, at a 1:1 volume ratio. Primary rat astrocytes were added to alginate solutions (4×10^6 cells/mL) with $CaCO_3$ (Ca^{2+}/COO^- molar ratio = 0.288) and δ-gluconolactone (GDL, Ca^{2+}/GDL molar ratio = 0.125), and the mixture was pipetted (20 μL) onto the wells (non-treated 48 well plate, Falcon). After crosslinking (1 h, 37 °C, 5 % CO_2), cell-laden 3D matrices were maintained in culture for three days, in DMEM or meningeal fibroblast CM medium (DIV 3). Afterwards, alginate discs were transferred to a 0.4 μm pore transwell system (BD Falcon) (with the help of a spoon) and added to OPC cultures. Co-cultures were maintained for additional six or eight days (DIV 9 or DIV 11).

For the experiments with the pharmacological inhibition of RhoA, pharmaceutical grade ibuprofen (purity >99 %, diluted in 70 % (*v*/v) ethanol) (kind gift from Dr. Sérgio Simões, Bluepharma) was added to the 3D cultured activated astrocytes (0.04 mM), at DIV 9 and maintained for 48 h (DIV 11).

2.4. Immunocytochemistry

Cells were fixed with 4 % (*w/v*) paraformaldehyde (Merck Milipore) diluted in phosphate buffered saline (PBS, pH 7.4, prepared with distilled water) for 20 min and further permeabilized and blocked with PBS containing 5 % (*v*/v) normal donkey serum (NDS) (Sigma) and 0.3 % (v/v) Triton X-100 (Sigma). Primary antibodies were diluted in PBS containing 1 % (v/v) NDS and 0.15 % (v/v) Triton X-100 and incubated overnight in a humid chamber at 4 °C. The following primary antibodies were used: rabbit anti-neuron-glial antigen 2 (anti-NG2) (1:250, Merck) and rat anti-myelin basic protein (anti-MBP) (1:100, AbD Serotec). Secondary antibodies Alexa-Fluor 488 anti-rat and 647 anti-rabbit were applied for 1 h at RT and subsequently treated for nuclear counterstaining at RT with Hoechst (Molecular Probes, 1:1000).

To evaluate cell culture purity, cells cultured on glass coverslips were fixed and stained for specific neuronal antibodies. Rabbit anti-IBA-1 (1:500, Wako) was used to detect microglia, rabbit anti-GFAP (1:1000, Abcam) for astrocytes, rat anti-MBP for OLs and mouse anti-βIII tubulin (1:500, BioLegend) for neurons.

2.5. Confocal laser scanning microscopy and image analysis

To evaluate the differentiation status of OPCs on microfibre samples at defined time-points, after immunocytochemistry and mounting with Fluoromount aqueous mounting medium (Sigma, F4680, refractive index 1.40) samples were observed under confocal laser scanning microscopes. For quantification of MBP, NG2 positive cells and MBP area, a TCS SP5 laser confocal inverted microscope (Leica Microsystems). Images were acquired using a HCX PL APO CS 40.0 × 1.30 OIL UV, with a resolution of 16 bits and in a sequential mode. A frequency of 400 Hz was applied with a unidirectional scan, a frame average of 3 and a line average of 2. An area of 387.5 × 387.5 μm (1024 × 1024, zoom factor 1) and a z-step size of 0.25 μm (z-size of 10 μm) were applied. MBP labelled with Alexa Fluor 488 nm was excited with a 488 nm laser line with a laser power of 38 % (set at 20 % Argon laser power), a gain of 745 and an offset of 0. Emission light was collected on a Leica PMT detector with a collection window of 497-556 nm. NG2 labelled with Alexa Fluor 647 nm was excited with a 633 nm laser line with a laser power of 30 %, a gain of 827 and an offset of −4. Emission light was collected on a Leica PMT detector with a collection window of 645-723 nm. Hoechst was excited with a 405 nm laser line with a laser power of 42 %, a gain of 631 and an offset of −3. Emission light was collected on a Leica PMT detector with a collection window of 427-494 nm. Fibre visualization was performed using transmitted light (gain 152, offset 1). For all the images, the pinhole size was 60.9 μm, calculated at 1 airy unit (AU) for 580 nm emission.

Cells positive for NG2 and MBP were manually counted using ImageJ (version 1.52u 17 March 2020, https://imagej.nih.gov/ij/notes.html) [28] from three P(TMC-CL) films from for every independent experiment (minimum 10 images per film). MBP area was estimated using image analysis tools. Images were segmented using a machine learning open-source software ilastik (version 1.3.3, https://www.ilastik. org/) [34], followed by further segmentation, detection of MBP objects and analysis using CellProfiler (version 3.1.9, https://cellprofiler.org) [35]. Results were analysed using Microsoft Excel (Microsoft Office 365). The area of the MBP staining is depicted as the number of MBP positive pixel per number of cells.

For visualization of the interaction of the OLs with the fibres a TCS SP8 confocal laser scanning microscope (Leica Microsystems) was used. Images were acquired using a HC PL APO CS2 63x/1.30 GLYC, with a resolution of 16 bits and in a sequential mode. A frequency of 700 Hz was applied with a unidirectional scan. An area of 81.73 × 81.73 μm with a pixel size of 80 nm (1024 × 1024, zoom factor 2.26) and a z-step size of 0.333 μm (z-size of 12 μm) were applied. MBP labelled with Alexa Fluor 488 nm was excited with a 488 nm laser line with a laser power of 0.5 % (set at 10 % Argon laser power), a gain of 15 and an offset of 0. Emission light was collected on a Leica HyD detector with a collection window of 508-571 nm. Hoechst was excited with a 405 nm laser line with a laser power of 6.13 %, a gain of 680 and an offset of −2. Emission light was collected on a Leica PMT detector with a collection window of 415-474 nm. Fibre visualization was performed using transmitted light (gain 664.7, offset 0.211). The pinhole size was 102.9 μm, calculated at 1 airy unit (AU) for 580 nm emission.

2.6. Stimulated emission depletion microscopy (STED)

To evaluate myelin wrapping around microfibers, OPCs at DIV 6 were fixed and stained as previously described. Secondary antibodies consisted of 635 anti-rat STAR Red (Aberion, diluted 1:100). Samples were mounted in 80 % (wt/v) glycerol medium (refractive index 1.44) and using a #1.5H cover glass (Zeiss). Image acquisition was carried on a Leica Stellaris 8 STED Falcon microscope (single point scanning confocal equipped with a fully motorized inverted Leica DMI8 microscope, a white light laser (WLL), Falcon and STED modalities) from Leica Microsystems. Images were acquired using a HC PL APO CS2 93x/1.30 glycerol immersion objective equipped with a correction collar. Images were recorded sequentially by frame scanning unidirectional at 400 Hz, with a line accumulation of 10, a pixel size of 31 nm, for an area size of 31.21 × 31.25 μm (1024 × 1024, zoom factor 4) and a z-step size of 0.3 μm (z size 10 μm). MBP labelled with Abberior STAR 635P was excited with a 633 nm laser line with a laser power of 2 %, and a gain of 10. Emission light was collected on a Leica HyDX4 detector (counting mode) with a collection window of 642–720 nm. The STED depletion was performed with a synchronized pulsed 775 nm (set at 85 %) and a depletion laser at 60 %. TauSTED was applied with the following parameters: Tau background: ON; Tau strength: 100; Denoise: 50. Hoechst was excited with a 405 nm laser line with a power of 2 % and a gain of 2. Emission was collected on a Leica HyD S1 detector (counting mode) with a collection window of 415–481 nm. The pinhole size was 110.2 μm, calculated at 1 airy unit (AU) for 580 nm emission. Due to fibre slightly autofluorescence, in the HyD S1 detector fibres were visualized.

2.7. Environmental scanning electron microscopy (ESEM)

After treatment with 4 % (*w/v*) paraformaldehyde solution diluted in PBS (pH 7.4,), OPCs cultured on P(TMC-CL) fibres were extensively rinsed with water. Samples were then imaged on a FEI Quanta 400FEG ESEM/EDAX Genesis X4M.

2.8. Focused ion-bean scanning electron microscopy (Fib-SEM)

Fibre samples with OPCs on top were firstly fixed with glutaraldehyde 2.5 % (*v*/v) diluted in 0.1 M cacodylate buffer for 2 h at RT. After two washing steps with 0.1 M cacodylate buffer, samples were incubated with osmium tetroxide at 4 % (wt/v) for 30 min at RT, washed twice with cacodylate buffer, followed by incubation with 1 % (wt/v) uranyl acetate (30 min, RT). Afterwards, fibres were dehydrated following a series of ethanol dilutions (50 %, 70 %, 90 % and 100 % (v/v) three times for 5 min each). Finally, samples were submerged in HMDS (Hexamethyldisilane, Sigma) and air-dried. Prior to scanning electron microscopy (SEM) samples were coated with 15 nm gold layer using sputter-coater (Q150RS, Quorum Technologies, UK). Cross-sectional milling was performed using cross-beam FIB-SEM microscopy (NEON 40EsB CrossBeam, Zeiss, Germany) with Ga-ion beam of 30 kV, 10 pA and aperture of 30 μm. The SEM imaging was performed at 3 kV with ESB detector. The acquired stack of cross-sectional SEM images was transformed into a 3D data volume with a voxel size of 3x3x9 nm and 4x4x12 nm for samples at DIV 6 and 8, respectively. The 3D reconstructions were performed using Avizo Fire (v6.3, Amira, U.S.A.) following the previous protocols [36–39].

2.9. Transmitted electron microscopy (TEM)

Samples were fixed by immersion in 2.5 % glutaraldehyde and 2 % paraformaldehyde in 0.1 M sodium cacodylate buffer (pH 7.4) solution for 5 days. After washing and 2 h in post-fixating 2 % osmium tetroxide in 0.1 M sodium cacodylate buffer (pH 7.4) solution, tissues were washed in buffer, incubated with 1%Uranyl acetate overnight, washed in buffer and dehydrated through graded series of ethanol, and embedded in Epon (EMS). Ultrathin sections were cut at 50 nm and prepared on an RMC Ultramicrotome (PowerTome, USA) using a diamond knife and recovered to 200 mesh Formvar Ni-grids, followed by 2 % uranyl acetate and saturated lead citrate solution. Visualization was performed at 80 kV in a (JEOL JEM 1400 microscope (Japan)) and digital images were acquired using a CCD digital camera Orious 1100 W (Tokyo, Japan).

2.10. RNA extraction and quantitative real-time polymerase chain reaction (qRT-PCR)

Total RNA from OPCs cultured on polymeric fibres was extracted using the Quick-RNA MiniPrep kit (Zymo Research) according to the

manufacturer's recommendations. Afterwards, one-step real time qRT-PCR was performed from 0.4 to 2 μg of RNA in a final volume of 20 μL using SYBR Green One Step qPCR Kit (Biotool), following producer's instructions. Analyses were performed on iCycler iQ5 (Biorad) in triplicates. The following gene sequences were designed and synthesized: *Mbp* sense primer: 5′ TGT CAC AAT GTT CTT GAA GAA 3′; *Mbp* anti-sense primer: 5′ GCT CCC TGC CCC AGA AGT 3′; *Ng2* sense primer: 5′ CAG TAC ACA CTA GCA CCG TC 3′; *Ng2* anti-sense primer: 5′ CCT CCT GGA CTA CCT CTA GC 3′; *Ywhaz* sense primer: 5′ ACG ACG TAC TGT CTC TTT TGG 3′; *Ywhaz* anti-sense primer: 5′ GTA TGC TTG CTG TGA CTG GT 3′.

To verify the specificity of the amplification and absence of primer dimer formation, corresponding melting curves were performed and analysed immediately after the amplification protocol. Non-specific products were not found in any case. *Ywhaz* was used as endogenous control to normalize the expression levels of genes of interest and the relative mRNA expression levels were calculated using the delta C_T ($2^{-\Delta\Delta CT}$) method [40].

2.11. Exosome isolation and characterization by transmission electron microscopy (TEM) and fluorescence-activated cell sorting (FACS)

Cell culture supernatants from monocultures of astrocytes embedded within alginate matrices cultured in the presence of DMEM or meningeal fibroblast CM medium were centrifuged twice for 10 min (firstly at 200 g and then at 500 g, both at 4 °C). Supernatants were frozen at −20 °C until further processing. After thawing, supernatants were spun down vertically at 2000*g*, 4 °C for 20 min and then centrifuged horizontally at 100,000*g* for 75 min. Finally, the supernatant was discarded, and the exosome pellet was re-suspended in 1 mL of PBS.

For transmission electron microscopy (TEM) morphological characterization, the exosomes were fixed overnight at 4 °C in 2.5 % (wt/v) glutaraldehyde/0.1 M sodium cacodylate buffer solution. Samples were then treated with 1 % (wt/v) OsO_4/0.1 M sodium cacodylate buffer, dehydrated through increasing concentration of ethanol solutions and then fixed in epoxy resin (EPON™). Ultrathin sections of 4 μm (ultramicrotome, LKB, Stockholm, Sweden) were prepared, stained with heavy metal solutions (1 % (wt/v) uranyl acetate and 1 % (wt/v) lead citrate) and analysed by TEM (Tecnai G12, FEI Company, Hillsboro, OR, USA) at acceleration voltage 100 kV. The image acquisition was performed by a video camera (Tietz, Tietz Video and Image Processing Systems GmbH, Gauting, 205 Germany) and an imaging software (TIA, FEI Company, Hillsboro, OR, USA).

Exosomes were also characterized by fluorescence-activated cell sorting (FACS) in terms of Cluster of Differentiation 81 (CD81) surface marker. Staining was performed for 30 min at 4 °C using conjugated primary CD81 antibodies (BD Pharmingen). Conjugated isotype-matching antibodies were used as negative controls. Cells were analysed with an Accuri C6 (BD Biosciences) and data were collected with FSC Express version 3 (*De Novo* Software). Exosomes were sorted by positivity for CD81 using a FACSAria III system (BD Biosciences). The purity of sorted populations was around 90 %.

Following isolation, exosomes in PBS were quantified through tuneable resistive pulse sensing (qNANO Gold, Izon Science Ltd., Cambridge, MA, USA). The analysis also provided data on size distribution of particles in the ADNV fraction. The nanopore (NP150, Izon Science Ltd., Cambridge, MA, USA) was stretched 49 mm wide using a digital calibre. During each measurement, the particle rate was maintained above 200 particles/min, and the total particle count surpassed 500 particles. The protein content was also established through Bradford assay with Pierce™ BCA Protein Assay Kit (Thermo Fisher Scientific, Waltham, MA, USA) following manufacturer's instructions. Absorbance was measured at 570 nm using multilabel plate reader Victor 3 (Perkin Elmer, Milano, Italy). The presence of exosomes specific protein has been performed by ELISA specific kit (Sigma). A table with detailed characteristics of the exosomes can be found in supplementary information (Supplementary Table S2).

2.12. Isolation of total RNA from exosomes and miScript ® miRNA PCR arrays

Exosomal RNA was isolated from previously purified exosomes using Total Exosome RNA and Protein Isolation Kit (Thermo Fisher Scientific). 100 ng of purified total RNA, including miRNAs, was extracted in 20 μL Elution Solution. Exosomal miRNA expression profiles were analysed using miScript miRNA PCR Arrays (Qiagen, MBRN-105Z) that investigated the expression of the 84 most abundantly expressed rat miRNAs related to inflammatory processes. For the first-strand cDNA synthesis, 200 ng of total RNA of each sample were reversely transcribed using the miScript II Reverse Transcription Kit (Qiagen), according to the user manual. The cDNA was pre-amplified with the miScript PreAMP PCR Kit, then mixed with QuantiTect SYBR Green PCR Master Mix, miScript Universal Primer, and RNase-free water. The PCR master mix was loaded in 25 μL aliquots across the microarray. The plate was run in a Rotor-Gene Q 100 (Qiagen) with the following thermal cycling conditions: initial activation step at 95 °C for 15 min, followed by 15 s at 94 °C for denaturation, 30 s at 55 °C for annealing, and 30 s at 70 °C for extension. The cycle number was set as 40 cycles. The relative expression of the miRNAs was analysed by the $2^{-\Delta\Delta CT}$ method in comparison to control samples present in the kit [41]. Fold changes >2 or <0.5 and *p*-values <0.05 were used as the thresholds for selecting differentially expressed miRNAs.

The expression of OL specific miRNAs was measured using miR-338, miR-219 and miR-125a3p specific primers (www.mirbase.org), using the small RNA U6 as an internal control for data normalization. The following sequences were designed and synthesized: miR-338 sense primer: 5′ TTG AAC T 3′, miR-338 anti-sense primer: 5′ CGC TAA GT 3′; miR-125a3p sense primer: 5′ AAA GTT TC 3′, miR-125a3p anti-sense primer: 5′ GGT TAC CTT TA 3′.

2.13. Statistical analysis

Statistical analysis was performed using the Graphpad Prism program (version 9). Statistical differences between groups were calculated based on one or two-way ANOVA followed by Sidak's multiple comparisons test for multiple comparisons. Gaussian distributions were tested using D'Agostino and Pearson normality tests. When Gaussian distribution could not be tested due to the lack of measurements or failed in the above-mentioned tests, non-parametric tests were performed (Kruskal-Wallis). Mann-Whitney tests were used in the case of unpaired *t*-tests. A *p*-value below 0.05 was considered statistically significant and data are shown either as mean ± standard deviation (SD) or mean ± standard error of the mean (SEM), as detailed.

3. Results

3.1. OPCs adhere, proliferate and differentiate on P(TMC-CL) fibres

Electrospun P(TMC-CL) fibres were found to have an average diameter of 0.64 ± 0.10 μm (Fig. 1A) and the fibre mats depicted a random orientation (Fig. 1B). Fibre diameter distribution values ranged from 0.2 μm to 3 μm, with only a very small percentage of the fibres having a diameter larger than 1.5 μm (Fig. 1A).

In the presence of appropriate culture medium containing factors fostering their development, OPCs were able to adhere, survive and differentiate (Fig. 2A) into MBP positive OLs when cultured on electrospun P(TMC-CL) fibres. After 8 days in culture, cells produced an exuberant network of processes that covered almost all the available fibres. As expected, the number of MBP positive cells increased overtime of culture from DIV2 to DIV8 but in comparison with traditional PLL-coated glass coverslips, the number of MBP and NG2 positive cells did not differ (Fig. 2B, C). Nevertheless, P(TMC-CL) fibres better support

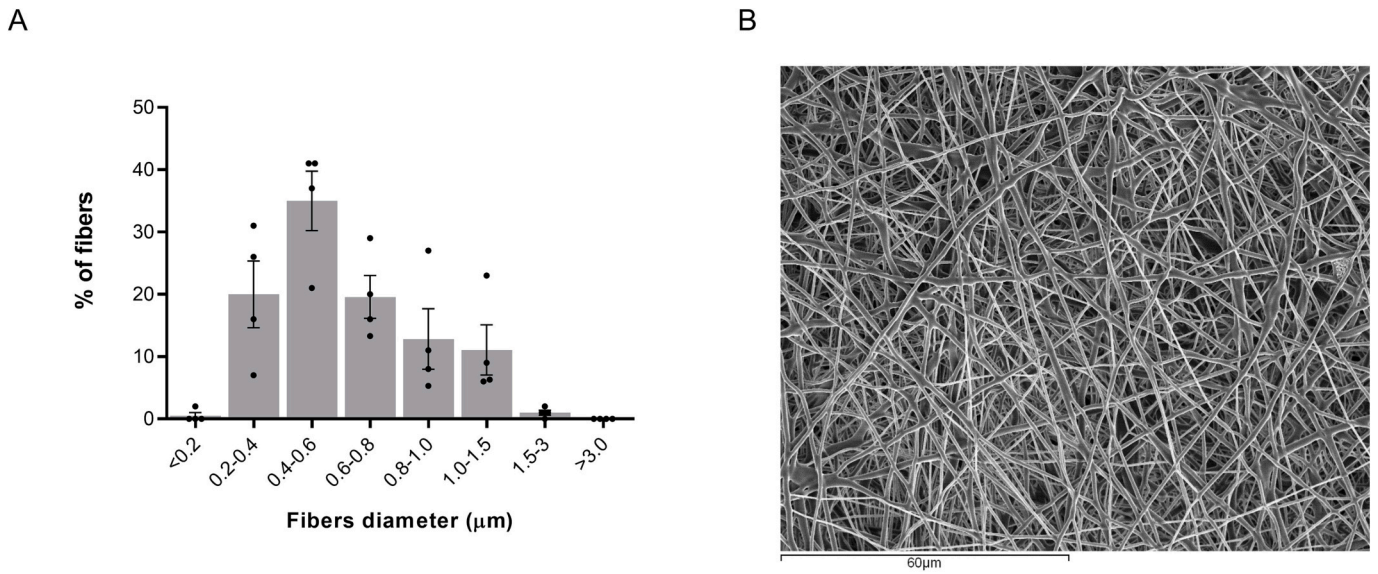

Fig. 1. P(TMC-CL) fibre morphology and characterization. A. P(TMC-CL) fibre diameter distribution ($n = 4$ independent P(TMC-CL) fibre films (30–300 microfibers analysed per film). Results show mean ± standard error of the mean (SEM). B. Representative scanning electron microscope image from the P(TMC-CL) fibres.

OPC differentiation compared with the traditional PLL coated glass control surfaces as OLs presented significantly higher area covered by MBP (Fig. 2D) and increased MBP mRNA expression (Fig. 2E).

Differentiated OLs were not only found to extend their processes along microfibres but also ensheathed them as depicted in Fig. 3 and Supplementary Fig. S2. A video of STED z planes and FIB-SEM reconstruction analysis can be found in Supplementary information (Supplementary Videos 1 and 2, respectively). It must be highlighted that this effect was observed without the need to coat the P(TMC-CL) fibres with adhesive molecules. TEM images reveal membrane wrapping around the microfibres (Fig. 3D).

3.2. Activated astrocytes inhibit OPC differentiation

To test the impact of astrocytic activity on oligodendrocyte differentiation, a co-culture protocol based on a transwell system was performed. Astrocytes were cultured within alginate hydrogels and activation induced by exposing them to meningeal fibroblast CM (Fig. 3), as previously described [18]. OPCs were seeded on P(TMC-CL) fibres and the co-culture was assembled at DIV 3. This time-point was chosen based on previous observations regarding the astrocytic peak of reactivity within alginate hydrogels [18].

Interestingly, only in the presence of activated 3D astrocyte cultures OL differentiation ability was inhibited (Fig. 5A), indicated by significant reduction of MBP gene expression and percentage of MBP positive cells (Fig. 5B, C). NG2 expression was not altered by the presence of activated astrocytes either at the transcription or protein level (Fig. 5B, C).

It is worth noting that there were no significant alterations in the expression of MBP and NG2 when OPC were cultured on fibres without astrocytes but in the presence of meningeal fibroblast CM. Hence, the observed decrease in oligodendrocyte differentiation was due to the activation of astrocytes and not to the culture medium by itself. Additionally, we found no differences on astrocytic viability in the presence of meningeal fibroblast CM (Supplementary Fig. S3) and on the number of cells counted *per* condition (Supplementary Fig. S4). This is indicative of no cell loss among the conditions.

3.3. Exosomes from astrocytes treated with conditioned medium contain miRNAs mediating inflammatory and demyelination processes

Extracellular vesicles (EVs) enriched in biological molecules as microRNAs (miRNA) are widely known by their role in mediating short and long-distance communications between cells [42]. To test if activated astrocytes produced EVs with differentially regulated miRNA we performed an exosome microarray analysis of medium derived from astrocytes cultured in DMEM or in CM. Exosomes were evaluated in terms of morphology by TEM analysis (size) and regarding the protein content and presence of typical surface markers (such as CD81, HSC70, CD63) (Supplementary Fig. S5, Table S2). Our microarray analyses showed a significant increase in the expression of miRNAs involved in the regulation of inflammatory pathways in astrocytes treated with CM compared to those in DMEM only (Fig. 6A).

This is indicative that activated astrocytes secrete exosomes that have a role in inflammation. The miRNAs identified in activated astrocytes regulate the expression of multiple classes of genes as transcription factors, growth factors, cytokines, interleukins, and chemokines (Fig. 6B). In activated astrocytes, we found significantly increased amounts of Rno-let-7b-5p, Rno-let-7c-5p, Rno-let-7e-5p, and the Rno-miR-181b-, and decreased amounts of Rno-miR-148b-3p, Rno-miR-16-5p, Rno-miR-203a-3p and Rno-miR-369 compared to control astrocytes grown in DMEM (Fig. 6C). These miRNAs are able to interfere with the expression of a multiple class of genes in the receptor cell (Supplementary Table S3).

Besides the inflammatory array, we have also searched for the presence of exosomes containing miRNAs that are involved in the differentiation of OLs. We focused our attention on miR-219, miR-338, as these are known to mediate the switch from proliferating to postmitotic oligodendrocytes [43,44], and miR-125a-3p that, when present at high level, blocks oligodendrocyte maturation and myelination [45–47]. Interestingly, we observed that both at DIV 3 and DIV 9 both miR-219 and miR-338 expression was significantly decreased in astrocytes grown in the presence of meningeal fibroblast CM. On the contrary, the expression of miR-125a-3p was significantly higher for activated astrocytes (treated with CM) in comparison with non-activated astrocytes (grown in DMEM) (Fig. 6D and E). This indicates that activated astrocytes secrete exosomes enriched in miRNA that inhibit myelination and non-activated astrocytes secrete exosomes with miRNA promoting myelination. It is important to note that exosome analysis was also

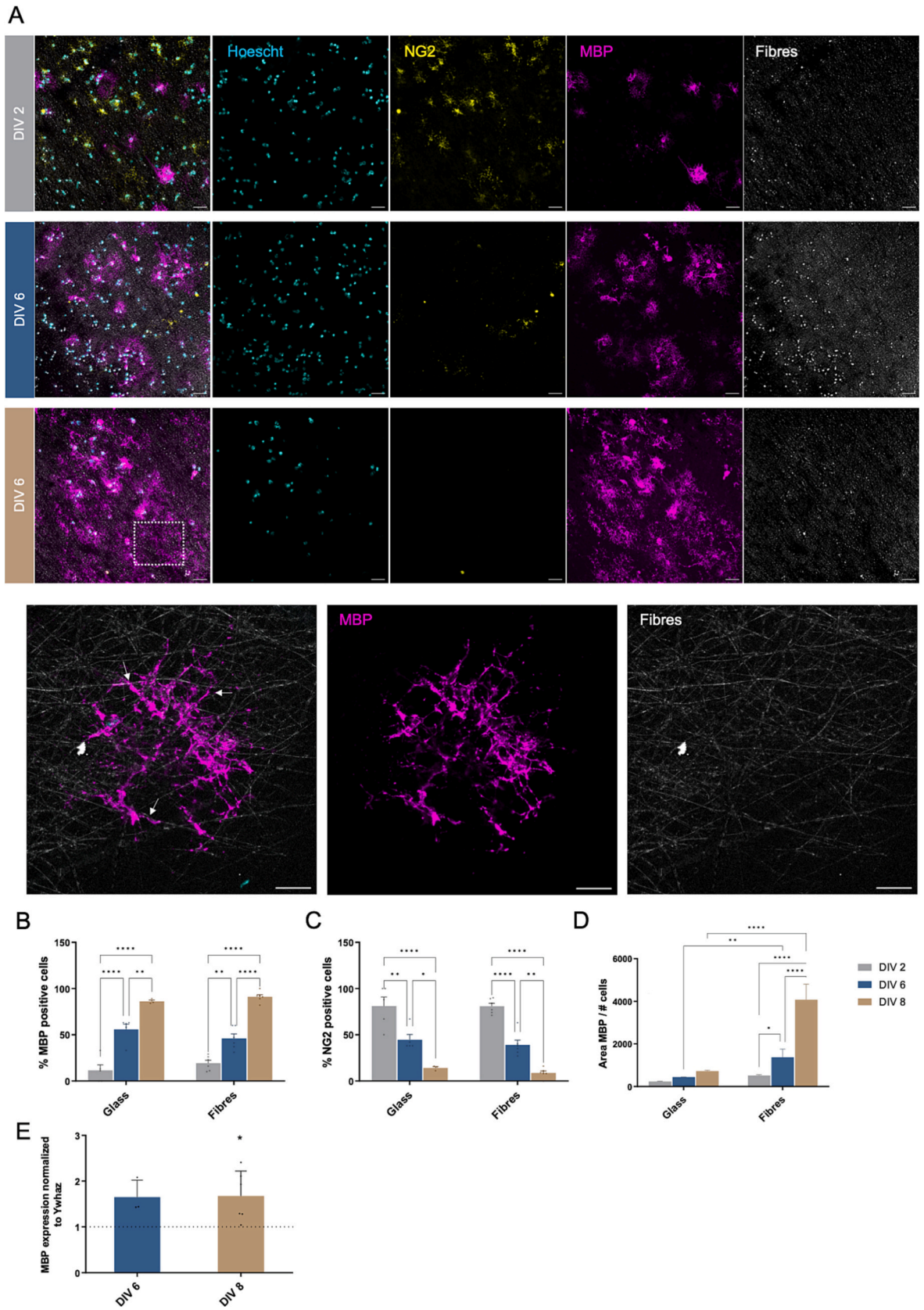

Fig. 2. Oligodendrocytes (OLs) cultured on P(TMC-CL) fibres. A. Representative images at DIV 2, 6 and 8, respectively. Scale bar indicates 30 μm. B. OLs' MBP expression when cultured on P(TMC-CL) fibres at DIV 6 and 8 in culture. mRNA levels were normalized to the glass control. Results show mean ± standard deviation ($n > 3$ independent experiments), asterisks represent statistical significance ($p \leq 0.05$). DIV8 is statistically significant compared to glass control. C. and D. Number of MBP and NG2 positive cells on glass coverslips or fibres throughout cell culture (DIV2, 6 and 8). Results show mean ± standard deviation ($n = 3$ independent experiments, two replicates per condition), asterisks represent statistical significance ($p \leq 0.05$).

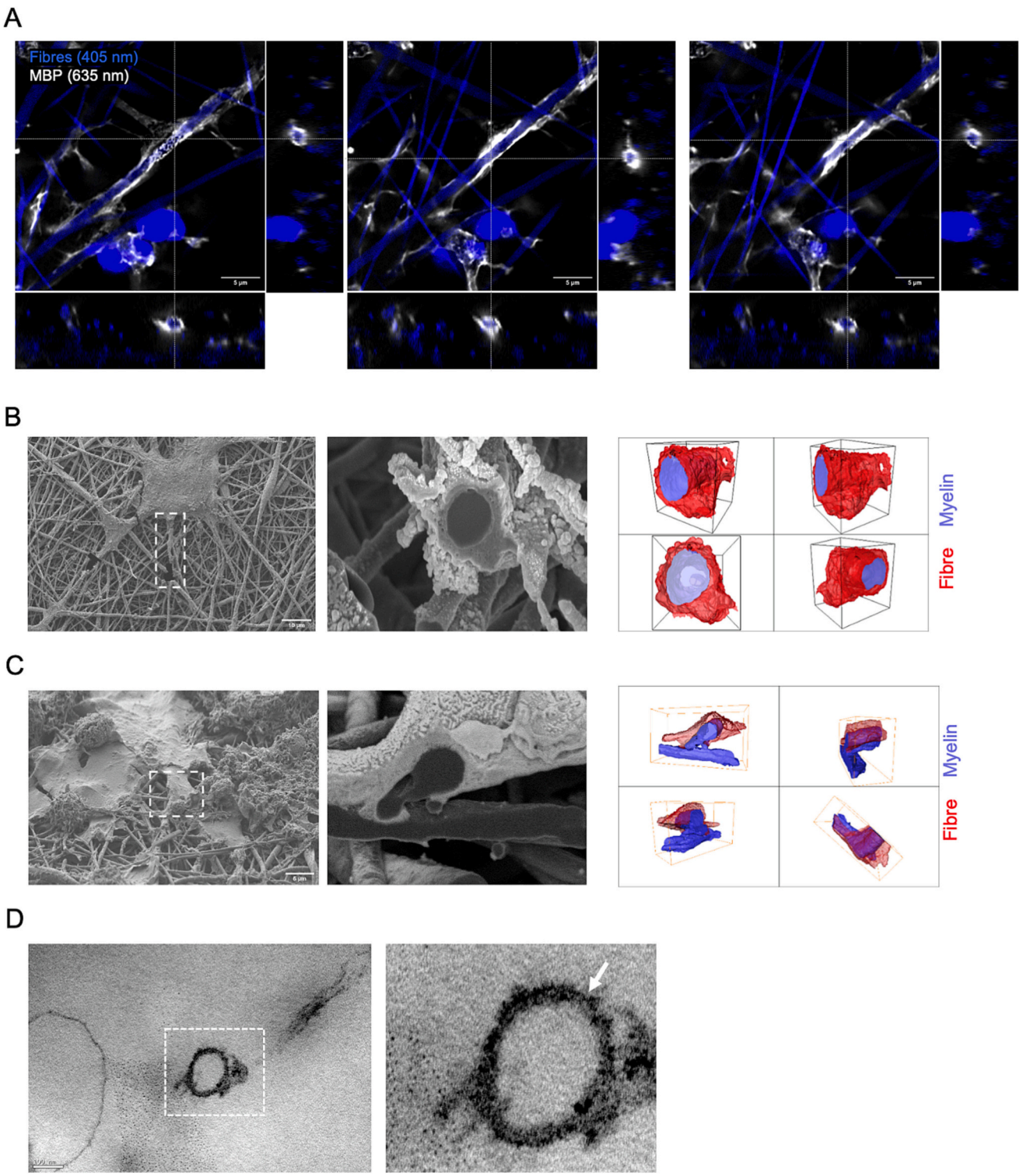

Fig. 3. Oligodendrocyte (OLs) membrane wrapping around P(TMC-CL) fibres. A. Super resolution microscopy (STED) images at DIV 6 of OLs interacting and wrapping the polymeric fibres. Images were taken from different z planes. Orthogonal views (XY on the right and XZ on the bottom) clearly demonstrate the wrapping of the myelin membrane around the fibres. Scale bar indicates 5 μm. For STED microscopy the fibres were visualized with the 405 nm laser as they presented some auto-fluorescence at that wavelength. B. and C. Focused ion beam-scanning electron microscopy (Fib-SEM) images of oligodendrocytes cultured in P (TMC-CL) fibres. I. SEM images where the cross-sectioning of the samples was applied using Fib-SEM. II. Cross-section of the individual P(TMC-CL) fibres wrapped by OLs. III. 3D reconstructions of P(TMC-CL) fibre (blue) wrapped by Ols (red) presented at four different angles. The size of the 3D tomography is 3.1 × 2.3 × 1 μm (D) and 4.1 × 3.1 × 1.5 μm. OLs were cultured for 6 and 8 days (D and E, respectively) on the fibres. D. Transmitted electron microscopy (TEM) images of oligodendrocytes cultured on the P(TMC-CL) fibres. Arrow points the cell membrane. Scale bar indicates 100 nm.

performed for conditions of oligodendrocytes cultured only in the presence of CM and DMEM but we were not able to detect their presence in the samples.

3.4. OPCs recover their differentiation ability after astrocyte phenotype rescue

To validate the impact of activated astrocytes on OL differentiation we decreased astrocytic reactivity with a RhoA inhibitor, ibuprofen [48,49]. We have previously shown that astrocyte activation was highly linked to RhoA modulation. In our previous study, by inhibiting RhoA activity by means of ibuprofen action we were able to rescue the astrocyte phenotype [18].

To understand if the ibuprofen addition to the cultures has an impact on the exosome production by astrocytes, we analysed the expression of the three target miRNA previously found to be altered in conditions where astrocytes where cultured with meningeal fibroblast CM (miR-219, miR-338, miR-125a-3p) (Fig. 7A). At DIV11, astrocytes cultured with meningeal fibroblast CM maintain the capacity of secreting exosomes containing high amounts of miR-338 and miR-219 but low levels of miR-125a-3p. Interestingly, when ibuprofen was added to the cultures of activated astrocytes we observed a clear tendency for the increasing of miR-338 and miR-219 (myelin promoters) and decreasing of miR-125a-3p (myelin inhibitor). It is important to highlight that we could not find exosomes for the media samples controls (DMEM, CM, DMEM + ibu and CM + ibu).

When the 3D astrocyte cultures co-cultured with OPCs were submitted to the same treatment for 48 h with ibuprofen (Fig. 4), the expression of MBP significantly increased compared with OPCs in the same conditions but not treated with ibuprofen (Fig. 7B–D). NG2 expression was not altered after the treatment (Fig. 7B–D). Of note, when ibuprofen was added for 48 h to OPC monocultures no effects on OPC differentiation ability were verified (Supplementary Fig. S6).

4. Discussion

The process of CNS myelination is complex and the mechanisms responsible for chronic remyelination failure have not yet been entirely explained. Although it is undeniable the existence of OPCs/OLs in the lesion sites [50,51], their involvement in the process of myelination has been the theme of recent debates and contradictions within the scientific community [2]. For long it was believed that cells surviving an episode of demyelination were unlikely the source of remyelinating cells as these are post-mitotic and cannot migrate to the lesion site. Several research studies showed the presence of neural progenitor cells (including OPCs) within the adult brain, which are capable of generate myelin sheaths and remyelinate denuded axons. Nevertheless, these evidences were based on rodent animal models. For humans, the degree of OPC generation in the adult brain is very limited as well as the presence of these cells in MS plaques is scarce [51–53]. Recently, a potential contribution of mature OLs to remyelination has been proposed [2,54,55]. Comparing MS patients with MS mice models, some differences within the OPC lineage were found. In MS patients, OPCs and intermediate cell stages were reduced while mature OLs were increased. In MS mice models the opposite was described. Despite these controversies, it is consensual that there are, both in animals and humans, functional differences in the myelin sheaths before and after the process of remyelination that ultimately result in loss of function. This clearly suggests the existence of regulatory mechanisms inhibiting myelination under pathological conditions.

Among all, ECM cues have been suggested as modulators of OPC and OL behaviour. Additionally, during demyelination in MS lesions the extensive remodelling of the environment, triggered not only by the myelin loss but also by microglia and astrocyte activation, can have a profound impact on remyelination processes [56,57]. Astrocytes specifically switch their quiescent phenotype to an activated state, creating a modified environment in which signaling molecules (growth factors, cytokines, and ECM constituents) are altered. Reactive astrocytes overexpress GFAP, vimentin, collagen type IV, chondroitin sulfate proteoglycans (CSPGs) and matrix metalloproteinases (MMP) as MMP-9. Ultimately, this process leads to the formation of a glial scar which is a highly inhibitory environment. This scar is formed by various cell types as astrocytes, meningeal fibroblasts, OLs and microglia [58].

Studying these phenomena has been a true challenge. The lack of an adequate (de)myelinating model in which one can specifically dig into the interactions between glial cell activation and OLs behaviour has led to results that are hardly comparable and confounding conclusions [57]. If on the one hand *in vivo* models are too complex to specifically dissect the crosstalk between these cells, on the other 2D traditional glass substrates do not mimic the (de)myelinating milieu features as stiffness, topography, and three-dimensionality. Approaches to mimic OL myelination processes with primary neurons have three major limitations: cost, time and reproducibility [59]. The emergence of the tissue engineering field where one can artificially reproduce the axonal features (with constructs that include for example microfibres or micropillars) revolutionized the way myelination is studied [57].

With electrospinning techniques, fibres can be rapidly produced in a standardized way with a range of chemical and physical properties depending on the polymer used. Furthermore, these 3D fibre mats can be configured into various diameters, orientations and even densities. The simplicity of this "artificial axon" system enables the monitoring of OL behaviour, namely differentiation capacity and membrane wrapping, in the absence of neuronal signals [20,21,60,61]. This model further allows the study of OL interactions with other CNS cells in the absence of neurons. Here we explore this "artificial axon" system to investigate if activated astrocytes directly affect OL differentiation capacity and, consequently if modulation of astrocyte reactivity may constitute an interesting therapeutic approach for remyelination purposes.

The majority of myelinated axons of the CNS are known to have between 0.2 and 2 μm of diameter with an average diameter of 1 μm [62,63]. As such, the selected P(TMC-CL) electrospun fibres, with a range of diameters between 0.2 μm and 3 μm, mimic a physiologically relevant mix of a CNS axon population. Remarkably, rat primary OPCs were able to directly adhere to bare polymeric fibres (Fig. 2). To the best

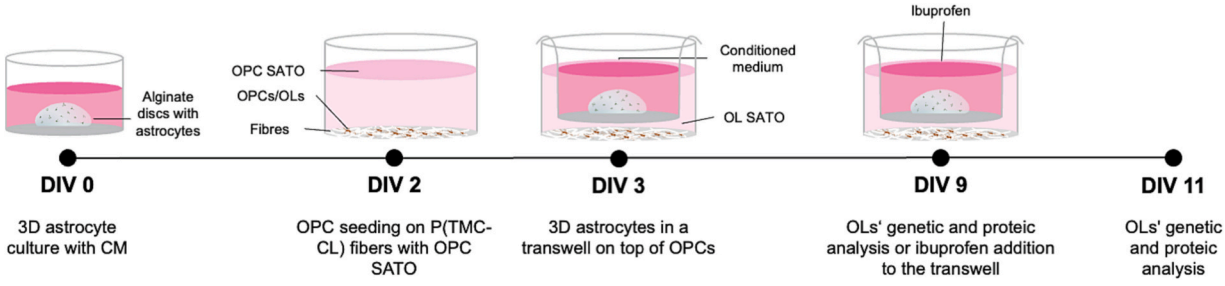

Fig. 4. Schematic representation of the experimental set-up. OPCs were cultured on top of P(TMC-CL) fibres with 3D astrocyte cultures (within alginate discs) on the upper chamber of a cell culture insert. 3D astrocyte cultures had been previously activated for 4 days, with meningeal fibroblast conditioned medium.

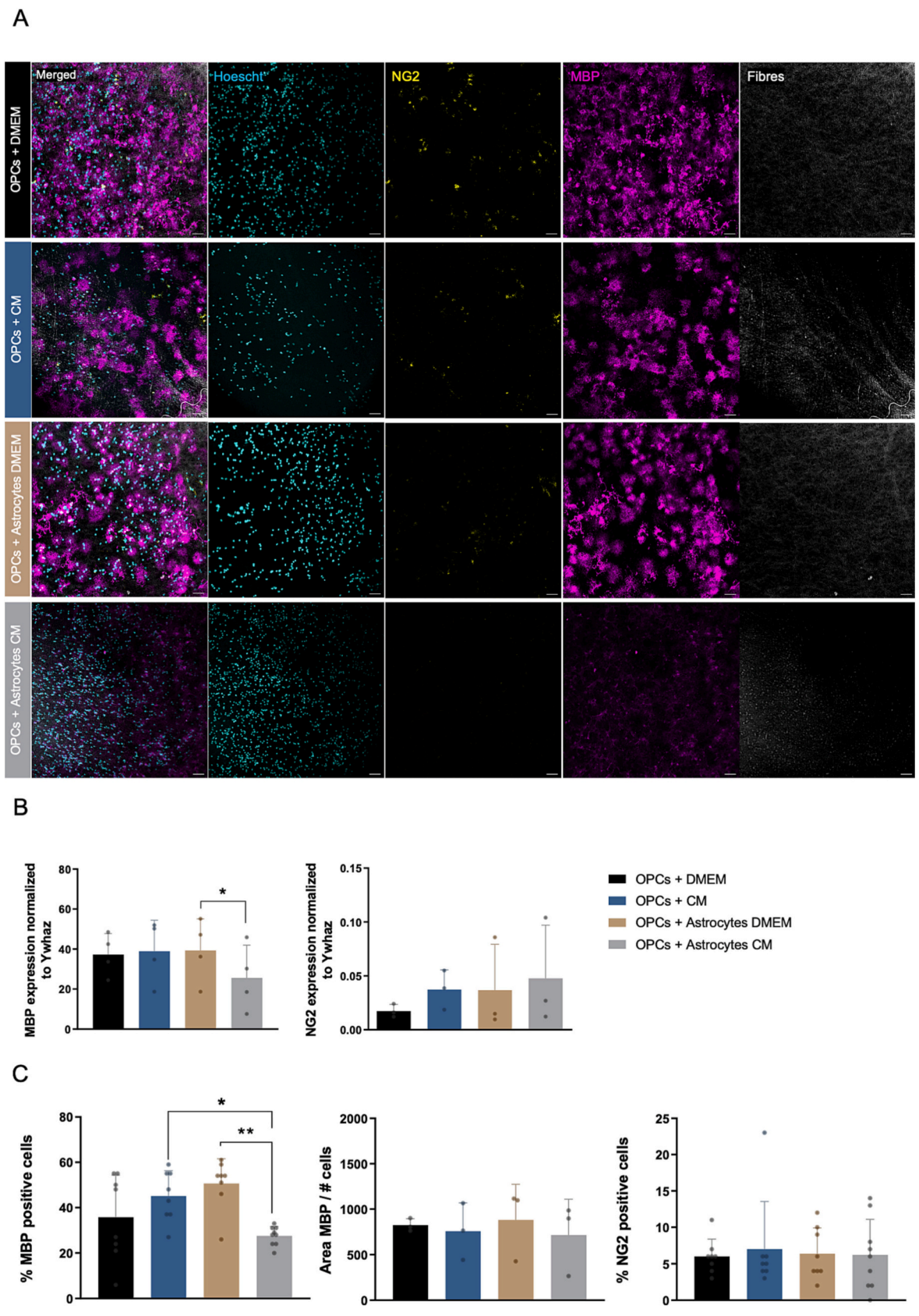

Fig. 5. Differentiation ability of oligodendrocytes (OLs) cultured on P(TMC-CL) fibres after co-culturing with astrocytes embedded within 3D alginate matrices. A. Representative images of OLs co-cultured with astrocytes at DIV 9 (maximum intensity z projections). Scale bar indicates 30 μm. B. mRNA levels of oligodendrocytes at DIV 9 in the presence of activated and non-activated astrocytes. *MBP* expression was normalized to *Ywhaz* housekeeping gene. Results show mean ± standard deviation ($n > 3$ independent experiments), asterisks represent statistical significance ($^{*}p \leq 0.05$, $^{**}p \leq 0.01$). C. Quantification of MBP, NG2 positive cells and MBP area at DIV 9 when oligodendrocytes were co-cultured with activated or non-activated astrocytes.

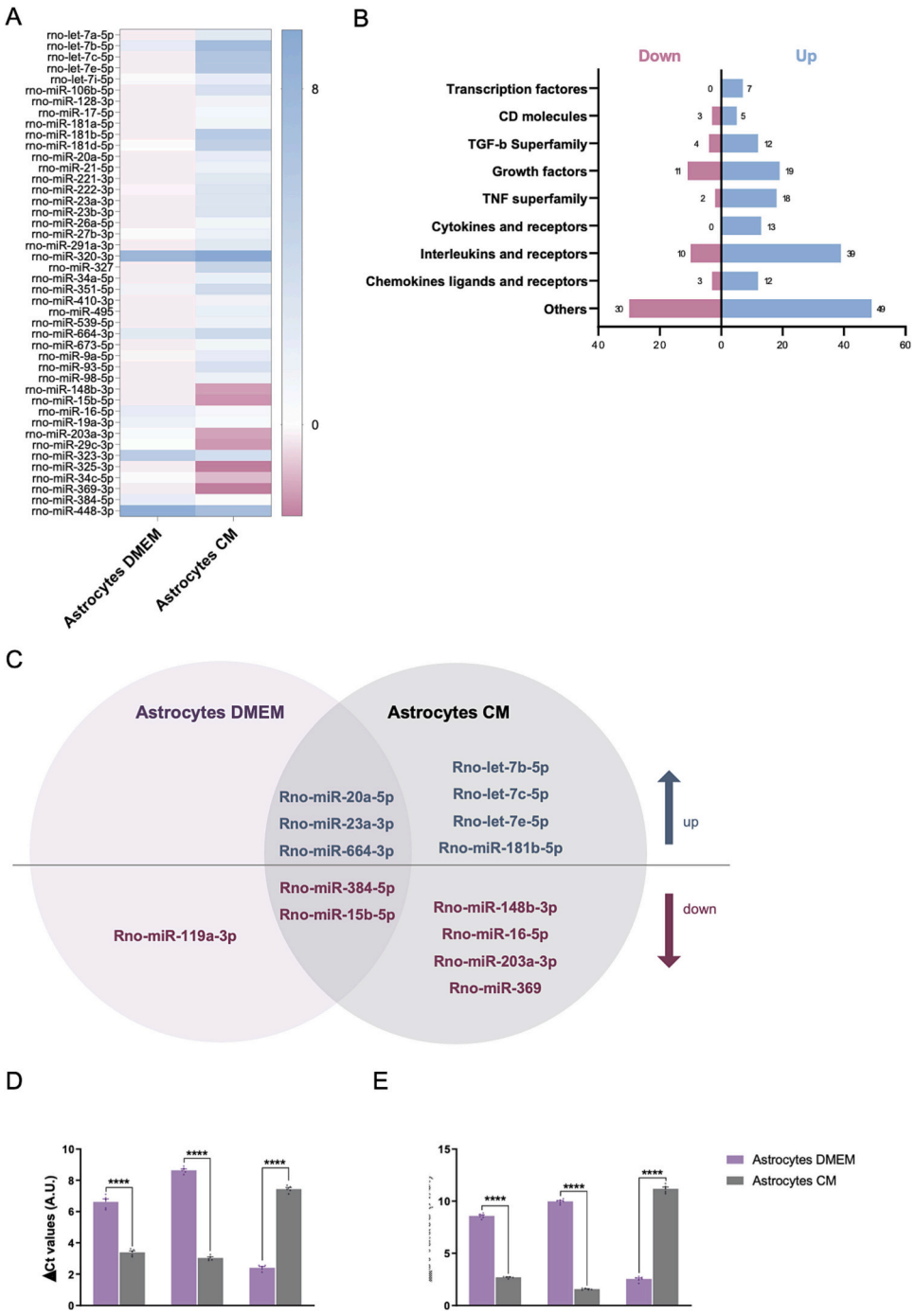

Fig. 6. Expression of microRNA (miRNA) in exosomes derived from monocultures astrocytes cultured in cell culture medium (DMEM) or conditioned medium (CM). A. Relative expression (log2) of inflammatory miRNA array in astrocytes cultured with DMEM or CM at DIV 9. B. Summary of the of classes of molecules that can be up- and down-regulated in miRNAs in astrocytes cultured with CM in comparison with astrocytes cultured in DMEM at DIV 9. C. Venn diagram with the more preeminent up- and down-regulated miRNAs in astrocytes cultured in DMEM and CM at DIV 9. D. and E. Expression levels of miR-338, miR-219 and miR-125a-3p in astrocytes cultured with DMEM and CM, at DIV 3 and DIV 9 respectively. Results show mean ± standard deviation ($n > 3$ independent experiments), asterisks represent statistical significance (****$p \leq 0.0001$).

of our knowledge, this is one of the first reports of the establishment of an artificial axon system without the need of adhesive coatings or chemical modifications with biological molecules. Noteworthy, some authors have even considered that the use of a coating was essential to promote myelin production in this model system [19,20,60,61,64,65]. The fact that these fibres do not need to be coated to support OPC adhesion and differentiation is of added value as several authors have already shown that many of the common coating molecules (*e.g.*, laminin 2) affect several signaling transduction pathways [66] in addition to those controlling cell adhesion. In fact, even poly-D-Lysine, which has been for long used to promote non-specific cell adhesion, can activate the phosphatidylinositol 3-kinase (PI3K) signaling pathway [67] or insulin mediated pathways [68], which are known to be involved in OL differentiation and CNS myelination [69,70]. Here, oligodendrocyte adhesion to the microfibres is likely to be regulated by protein adsorption only produced by the cells. Oligodendrocytes can produce some ECM proteins like collagen (semaphorin 4D) and proteoglycans (brevican, aggrecan, tenascins) that can adsorb to the polymer network and therefore promote oligodendrocyte adhesion [71].

Our platform revealed to be crucial to obtain significant myelination after a short period of time with an accelerated differentiation program in comparison with traditional glass surfaces (Fig. 2), suggesting an important role of the physical cues for processes of OL differentiation and myelin production. These results also highlight that although neurons undoubtedly play an important role in the myelination process, they are not crucial for the onset of OL differentiation and myelin expression. Additionally, in an *in vitro* context, the presence of an adhesive substrate is also not essential for myelination to occur.

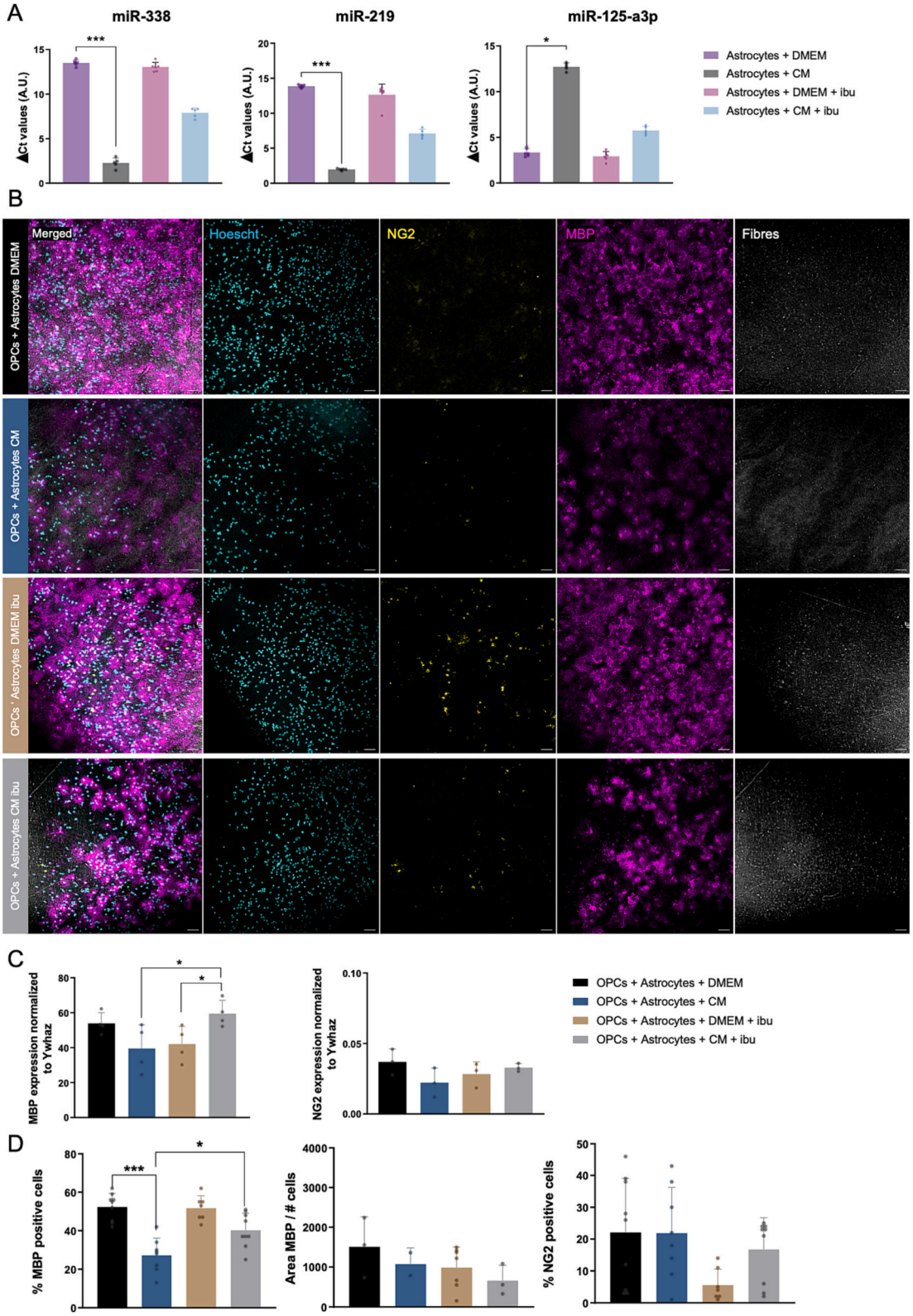

Fig. 7. Effects of ibuprofen (ibu) on the rescue of the oligodendrocyte (OL) phenotype. A. Exosome production by astrocytes cultured in the presence of ibu. B. Representative images of OLs after co-culturing with astrocytes in the presence of cell culture medium (DMEM) meningeal fibroblast conditioned medium (CM) at DIV 11 and after astrocytic treatment with ibuprofen (maximum intensity z projections). C. Quantification of MBP, NG2 positive cells and area occupied by MBP before and after ibuprofen treatment at DIV 11. Results show mean ± SEM ($n > 3$ independent experiments), asterisks represent statistical significance ($*p \leq 0.05$, $***p \leq 0.001$). D. mRNA levels of oligodendrocytes after treatment with ibuprofen. *mbp* and *ng2* expression was normalized to levels of the housekeeping gene *Ywhaz*. Results show mean ± standard deviation (n > 3 independent experiments), asterisks represent statistical significance ($*p \leq 0.05$).

To test the hypothesis that astrocyte phenotype plays a direct role in OPC differentiation, OPCs were cultured in the presence of a tissue engineered glial scar, in which astrocytes are in an activated state (Fig. 3). Astrocyte reactivity was achieved, as we have previously described [18], by culturing astrocytes within 1 % (*w/v*) alginate-based hydrogels in the presence of meningeal fibroblast CM. In this experimental setting astrocyte increased the expression of astrogliosis hallmark genes including *Gfap* and *Vimentin*, and increased production of ECM molecules such as CSPG and collagen IV. Here OPCs were cultured on P(TMC-CL) fibres in the presence of astrocytes cultures within 3D hydrogels maintained in the top compartment of a transwell system. Our data indicates that activated astrocytes significantly impair OL differentiation ability when compared to control astrocytes (Fig. 4). This effect was not due to conditioned medium *per se* as the differentiation state of OL remained unchanged when these were cultured in the presence of CM but without astrocytes. Furthermore, very little astrocyte cell death was observed at all times in the different cell cultures, indicating that cell debris may not have been the reason for the impairment of OL differentiation. Moreover, the expression levels of progenitor marker NG2 did not differ between conditions. We therefore hypothesize that co-culture with activated astrocytes impairs the OLs maturation process, even in differentiation culture conditions, most probably due to astrocytes secreted products as there was no direct contact between both cell types.

Intercellular communication occurs either through direct contact of molecules on cell surfaces; secretion of soluble molecules to distant cells; or *via* extracellular vesicle release (exosomes) [72]. Here, we show that activated astrocytes release exosomes with a distinct miRNA content in relation to those of non-activated astrocytes. miRNA is a class of short non-coding RNAs with ~22 nucleotides regulating a multitude of biological processes by blocking translation of mRNAs through targeting their untranslated and coding regions. By controlling multiple aspects of cellular development and homeostasis, including cell-fate determination and differentiation, miRNAs are powerful post-transcriptional regulators [73]. Here we report remarkable differences in miRNA regulating inflammatory processes with a high number of miRNA being upregulated in astrocytes cultured with CM (Fig. 6). Among all, the genes that some of these miRNAs can silence include the *Osmr* and the *Tr1* (Supplementary Table S2) which were already proved to be positively involved in the regulation of the OL differentiation [74,75]. Additionally, we found strong differences in the expression of miRNAs that are already known to be involved in myelination processes (miR-219, miR-338 and miR-125-a3p) in both conditions. miR-219 and miR-338 are critical for OL differentiation, being miR-219 actions exacerbated by miR-338. These miRNAs act through suppression of OL differentiation inhibitors, including Lingo1, Etv5, PDGFRα, Sox6, and Zfp238 [43,44,76]. On the opposite, miR-125a-3p was found to be expressed at higher levels in activated astrocytes. When present at high levels, this miRNA can block the OL differentiation and myelination [45–47]. Due to its recent discovery, the targets of miR-125a-3p in oligodendroglial cells are still largely unknown. Notwithstanding, this miRNA is able to bind and inhibit the action of Fyn [77], a crucial kinase to induce localized translation of MBP mRNA at sites of axon-glia contact [78]. Fyn kinase in turn activates small GTPases such as Rac1 and Cdc42 which are upregulated during differentiation. [79,80]. Additionally, several ECM adhesion molecules such as catenin, collagens, integrins, laminins and MMPs can be altered by miR-125a-3p. The role of the ECM molecules in OL differentiation and maturation is well established: for instance, disruption of integrin-ECM connection leads to aberrant processes growing and myelination. miR-125a-3p is also capable of altering genes regulating the formation of gap junctions, such as Lpar1 (surface receptor), MAPKs and PKC (intracellular kinases) and Cx47, Cx32 and Cx29 (connexins) [47], whose fundamental roles for OL myelination are well established [81–84]. Finally, another direct target of miR-125a-30 is neuregulin 1 (NRG1), which is a trophic factor that regulates OPC migration and the extension of OL myelination during development [85].

Others have shown that astrocytes support OL functions *via* EVs [86] and that upon activation astrocytes change the secretion and the cargo of EVs with a striking impact on neuronal activity [72,87,88]. Nonetheless, to the best of our knowledge, this is the first time that the secretion of exosomes by activated astrocytes is directly linked to OL differentiation impairment. Interestingly, miRNAs' expression can be a promising diagnostic tool to detect early demyelinating lesions. In fact, miR-125a-3p was found upregulated in active MS patients' lesions [46]. On the other hand, differentially expressed miRNAs by other glial cells as astrocytes can be considered a novel therapeutical avenue to overcome myelin damage in demyelinating conditions.

The role of astrocytes on demyelinating pathologies has been the theme of intense debates over the last years. While some reports support that the astrogliosis and the glial scar promote regeneration and remyelination [89,90] by function as a physical barrier to damage, many authors defend the negative role of reactive astrocytes on OL differentiation and myelin ensheathment [91,92]. For instance, during astrogliosis, activated astrocytes are known to express high amounts of MMPs like MMP-2 that degrades MBP [93]. Suppression of MMPs in the EAE mouse model attenuates the effects of demyelination [94]. Additionally, CSPGs are upregulated in demyelinated MS lesions and were shown to have a negative effect in OL maturation and myelination [95,96]. Moreover, activated astrocytes secrete various cytokines as tumour necrosis factor alpha (TNF-α) which was proven to induce OPC apoptosis and inhibit differentiation after spinal cord injury [97]. Bone morphogenic proteins, highly expressed by reactive astrocytes also impair OPC differentiation [98]. Furthermore, the secretion of many altered ECM proteins during astrogliosis has a tremendous impact on the mechanical properties of the lesioned tissue. At the same the biophysical characteristics of the environment can alter astrocytic reactivity. We have previously shown that astrocytic activation is modelled by the mechanical properties of the environment and that modulating mechanosensing pathways this process can be reverted.

To confirm the crucial role of astrogliosis on OL myelination we reduced astrocytic reactivity with a RhoA inhibitor, ibuprofen, a non-steroidal anti-inflammatory drug that blocks RhoA levels [48,49]. Previously, we demonstrated that RhoA is a pivotal modulator of astrocyte behaviour, and its chemical inhibition with ibuprofen reduces astrogliosis by recovering normal astrocyte phenotype [18]. Others have also proven that ibuprofen can ameliorate the astrocytic inflammatory environment characterized by extensive production of GFAP, oxygen reactive species and TNF-α [99–101]. Here, the treatment of reactive astrocytes with ibuprofen for 48 h reverted the secretion of exosomes containing miRNAs capable of regulating of myelin. While without ibuprofen, astrocytes express low levels of miR-219 and miR-338 (OL differentiation inducers) and high levels of miR-125a-3p, after treatment with this drug this scenario was inverted. Consequently, the inhibitory effect on OL differentiation was overcome, with protein and expression of MBP mRNA being significantly higher than non-treated samples (Fig. 7). It is important to highlight that ibuprofen did not affect OL differentiation (Supplementary Fig. S6). The positive effects of ibuprofen on myelination have been also demonstrated by others: in a model of spinal cord injury this drug reduced OL death and increased myelination [102] and more recently in a hypomyelination model, undifferentiated states of OPCs were reversed after ibuprofen treatment [103].

Altogether, these results reinforce astrocytes' role in CNS myelination processes and highlight astrocytes' potential as a therapeutic target in demyelinating diseases.

For the first time, a co-culture system based on 3D biomaterials was established to study the crosstalk between astrocytes and oligodendrocytes. To the best of our knowledge, up until now studies on the interaction of these glial cells were made using complex *in vivo* models. Co-culture systems of astrocytes and oligodendrocytes are scarce in the literature and rely merely on the plating of these two type of cells in

substrates that do not resemble the natural environment of these cells [104,105]. Additionally, none of the systems reported in the literature showed capacity to model astrogliosis phenotypes and therefore studying this regarding oligodendrocyte differentiation.

5. Conclusions

In this study, we have established a novel model of (de)myelination taking advantage of CNS mimicking-biomaterials and allowing the specific study of astrocyte-OL crosstalk. Within this model, reactive astrogliosis, achieved through exposing these cells to meningeal fibroblast CM and modelled by the hydrogel network mechanical properties, significantly inhibited OL differentiation. Additionally, the pharmacological inhibition of astrogliosis-mediated mechanosensing pathways enabled the recovery of OL differentiation ability. We also have strong evidence that the crosstalk between these glial cells is partially mediated by miRNAs inside EVs (exosomes). This knowledge is relevant in the context of demyelinating neurodegenerative diseases, such as MS, where astrogliosis is known to occur together with remyelination failure.

We have further been able to uncouple axonal signaling from OL differentiation and myelination events, reinforcing the importance of physical cues for the myelination process. Additionally, the proposed *in vitro* artificial axon system is advantageous for studies aiming to dissect the molecular mechanisms of myelination. The removal of the neuronal cell contribution to the process allows an individual monitorization of OL branching and ensheathment.

Finally, our co-culture system allows for the easy screening of drugs or therapeutic molecules potentially promoting (re)myelination processes and constitutes an advance to the design of *in vitro* CNS suitable models.

Supplementary data to this article can be found online at https://doi.org/10.1016/j.bioadv.2023.213429.

CRediT authorship contribution statement

A. P. Pêgo, D. N. Rocha, E. D. Carvalho and J. B. Relvas contributed to the conceptualization and design of the work hereby presented. Data collection was conducted by D. N. Rocha, E. D. Carvalho, L. R. Pires, C. Gardin, I. Zanolla, P. K. Szewczyk, C. Machado and R. Fernandes. Data analysis and interpretation was carried out by D. N. Rocha, E. D. Carvalho, P. K. Szewczyk, U. Stachewicz, R. Fernandes, B. Zavan, and A. P. Pêgo. The manuscript draft preparation was conducted by E. D. Carvalho and D. N. Rocha and critical revision of the article by A. P. Pêgo and J. B. Relvas. A. P. Pêgo assured and managed the funding. All authors reviewed the results and approved the final version of the manuscript.

Declaration of competing interest

None of the authors or suggested reviewers have any conflict of interest, financial or otherwise.

Data availability

Data will be made available on request.

Acknowledgements

A.P. Pêgo acknowledges the funding from projects UTAPEXPL/NTec/0057/2017 (FCT – Portuguese Foundation for Science and Technology – UT Austin Portugal Program) and GRANT13074566 - Award FA9550-20-1-0417 (Air Force Office of Scientific Research, USA).

The authors acknowledge the *Centro de Materiais da Universidade do Porto* (CEMUP) for ^{1}H NMR, SEM (polymer fibres) and ESEM analyses, as well as Dr. J. Coelho (Universidade de Coimbra) for GPC measurements.

The authors acknowledge the support of the i3S Scientific Platforms Bioimaging, Advanced Light Microscopy (ALM) and Histology and Electron Microscopy (HEMS), members of the PPBI (PPBI–POCI-01-0145-FEDER-022122).

The authors acknowledge Joana Bravo from Addiction Biology group (i3S) for kindly sharing spared rat primary oligodendrocytes and astrocytes cultures whenever available.

U. Stachewicz thanks funding from the OPUS 17 project grant provided by the National Science Centre in Poland No 2019/33/B/ST5/01311 supporting SEM and FIB-SEM imaging (OLs on polymeric fibres).

E. D. Carvalho acknowledges the support by FCT – Portuguese Foundation for Science and Technology for her Ph.D. (SFRH/BD/140363/2018) fellowship.

All authors acknowledge the COST Action CA16122 - Biomaterials and advanced physical techniques for regenerative cardiology and neurology (BIONECA).

References

[1] C. Walton, et al., in: third edition.Rising Prevalence of Multiple Sclerosis Worldwide: Insights From the Atlas of MS, 26, Mult Scler, 2020, pp. 1816–1821.
[2] R.J.M. Franklin, J. Frisén, D.A. Lyons, Revisiting remyelination: towards a consensus on the regeneration of CNS myelin, Semin. Cell Dev. Biol. 116 (2021) 3–9.
[3] I.D. Duncan, et al., The adult oligodendrocyte can participate in remyelination, Proceedings of the National Academy of Sciences 115 (50) (2018) E11807–E11816.
[4] L. Bierhansl, et al., Thinking outside the box: non-canonical targets in multiple sclerosis, Nat. Rev. Drug Discov. 21 (8) (2022) 578–600.
[5] M. Yamada, et al., The molecular regulation of oligodendrocyte development and CNS myelination by ECM proteins, Front. Cell. Dev. Biol. 10 (2022), 952135.
[6] J.A. Cossins, et al., Enhanced expression of MMP-7 and MMP-9 in demyelinating multiple sclerosis lesions, Acta Neuropathol. 94 (6) (1997) 590–598.
[7] A. Weaver, et al., An elevated matrix metalloproteinase (MMP) in an animal model of multiple sclerosis is protective by affecting Th1/Th2 polarization, FASEB J. 19 (12) (2005) 1668–1670.
[8] D.N. Rocha, et al., Mechanotransduction: exploring new therapeutic avenues in central nervous system pathology, Front. Neurosci. 16 (2022), 861613.
[9] M.M. Urbanski, M.B. Brendel, C.V. Melendez-Vasquez, Acute and chronic demyelinated CNS lesions exhibit opposite elastic properties, Sci. Rep. 9 (1) (2019) 999.
[10] T.A. Watkins, et al., Distinct stages of myelination regulated by gamma-secretase and astrocytes in a rapidly myelinating CNS coculture system, Neuron 60 (4) (2008) 555–569.
[11] A. Sorensen, et al., Astrocytes, but not olfactory ensheathing cells or schwann cells, promote myelination of CNS axons in vitro, Glia 56 (7) (2008) 750–763.
[12] T. Ishibashi, et al., Astrocytes promote myelination in response to electrical impulses, Neuron 49 (6) (2006) 823–832.
[13] M. Absinta, et al., A lymphocyte–microglia–astrocyte axis in chronic active multiple sclerosis, Nature 597 (7878) (2021) 709–714.
[14] R. Masvekar, et al., Cerebrospinal fluid biomarkers link toxic astrogliosis and microglial activation to multiple sclerosis severity, Mult. Scler. Relat. Disord. 28 (2019) 34–43.
[15] R.P. Gorter, W. Baron, Recent insights into astrocytes as therapeutic targets for demyelinating diseases, Curr. Opin. Pharmacol. 65 (2022), 102261.
[16] T. Kuhlmann, et al., An updated histological classification system for multiple sclerosis lesions, Acta Neuropathol. 133 (1) (2017) 13–24.
[17] Y. He, X. Liu, Z. Chen, Glial scar-a promising target for improving outcomes after CNS injury, J. Mol. Neurosci. 70 (3) (2020) 340–352.
[18] D.N. Rocha, et al., Extracellular environment contribution to astrogliosis-lessons learned from a tissue engineered 3D model of the glial scar, Front. Cell. Neurosci. 9 (2015) 377.
[19] M.E. Bechler, L. Byrne, C. Ffrench-Constant, CNS myelin sheath lengths are an intrinsic property of oligodendrocytes, Curr. Biol. 25 (18) (2015) 2411–2416.
[20] S. Lee, et al., A culture system to study oligodendrocyte myelination processes using engineered nanofibers, Nat. Methods 9 (9) (2012) 917–922.
[21] S. Lee, et al., A rapid and reproducible assay for modeling myelination by oligodendrocytes using engineered nanofibers, Nat. Protoc. 8 (4) (2013) 771–782.
[22] A.P. Pêgo, et al., Adhesion and growth of human Schwann cells on trimethylene carbonate (co) polymers, J. Biomed. Mater. Res. A 67 (3) (2003) 876–885.
[23] D.N. Rocha, et al., Poly(trimethylene carbonate-co-ε-caprolactone) promotes axonal growth, PLoS ONE 9 (2) (2014), e88593.
[24] A.P. Pêgo, et al., Copolymers of trimethylene carbonate and ε-caprolactone for porous nerve guides: synthesis and properties, J. Biomater. Sci. Polym. Ed. 12 (1) (2001) 35–53.
[25] A.P. Pego, et al., Influence of catalyst and polymerization conditions on the properties of 1, 3-trimethylene carbonate and ε-caprolactone copolymers, Macromol. Chem. Phys. 204 (5–6) (2003) 747–754.
[26] L.R. Pires, et al., Ibuprofen-loaded poly (trimethylene carbonate-co-ε-caprolactone) electrospun fibres for nerve regeneration, J. Tissue Eng. Regen. Med. 10 (3) (2016) E154–E166.

[27] L.R. Pires, et al., Ibuprofen-loaded poly(trimethylene carbonate-co-epsilon-caprolactone) electrospun fibres for nerve regeneration, J. Tissue Eng. Regen. Med. 10 (3) (2013) E154–E166.
[28] C.A. Schneider, W.S. Rasband, K.W. Eliceiri, NIH image to ImageJ: 25 years of image analysis, Nat. Methods 9 (7) (2012) 671–675.
[29] Y. Chen, et al., Isolation and culture of rat and mouse oligodendrocyte precursor cells, Nat. Protoc. 2 (5) (2007) 1044–1051.
[30] K.D. McCarthy, J. de Vellis, Preparation of separate astroglial and oligodendroglial cell cultures from rat cerebral tissue, J. Cell Biol. 85 (3) (1980) 890–902.
[31] B.E. Güler, J. Krzysko, U. Wolfrum, Isolation and culturing of primary mouse astrocytes for the analysis of focal adhesion dynamics, STAR Protoc 2 (4) (2021), 100954.
[32] D.M. Skytt, et al., Characterization of primary and secondary cultures of astrocytes prepared from mouse cerebral cortex, Neurochem. Res. 35 (12) (2010) 2043–2052.
[33] F.R. Maia, et al., Hydrogel depots for local co-delivery of osteoinductive peptides and mesenchymal stem cells, J. Control. Release 189 (2014) 158–168.
[34] S. Berg, et al., Ilastik: interactive machine learning for (bio)image analysis, Nat. Methods 16 (12) (2019) 1226–1232.
[35] C. McQuin, et al., Cell profiler 3.0: next-generation image processing for biology, PLoS Biol. 16 (7) (2018), e2005970.
[36] U. Stachewicz, et al., 3D imaging of cell interactions with electrospun PLGA nanofiber membranes for bone regeneration, Acta Biomater. 27 (2015) 88–100.
[37] U. Stachewicz, et al., Pore shape and size dependence on cell growth into electrospun fiber scaffolds for tissue engineering: 2D and 3D analyses using SEM and FIB-SEM tomography, Mater. Sci. Eng. C 95 (2019) 397–408.
[38] S. Metwally, et al., Surface potential and roughness controlled cell adhesion and collagen formation in electrospun PCL fibers for bone regeneration, Mater. Des. 194 (2020), 108915.
[39] P.K. Szewczyk, et al., Surface-potential-controlled cell proliferation and collagen mineralization on electrospun polyvinylidene fluoride (PVDF) fiber scaffolds for bone regeneration, ACS Biomaterials Science & Engineering 5 (2) (2019) 582–593.
[40] K.J. Livak, T.D. Schmittgen, Analysis of relative gene expression data using real-time quantitative PCR and the 2(-Delta Delta C(T)) method, Methods 25 (4) (2001) 402–408.
[41] M.W. Pfaffl, A new mathematical model for relative quantification in real-time RT-PCR, Nucleic Acids Res. 29 (9) (2001), e45.
[42] T. Gharbi, Z. Zhang, G.Y. Yang, The function of astrocyte mediated extracellular vesicles in central nervous system diseases, Front. Cell Dev. Biol. 8 (2020), 568889.
[43] H. Wang, et al., miR-219 cooperates with miR-338 in myelination and promotes myelin repair in the CNS, Dev. Cell 40 (6) (2017) 566–582.e5.
[44] J.C. Dugas, et al., Dicer1 and miR-219 are required for normal oligodendrocyte differentiation and myelination, Neuron 65 (5) (2010) 597–611.
[45] D. Lecca, et al., MiR-125a-3p timely inhibits oligodendroglial maturation and is pathologically up-regulated in human multiple sclerosis, Sci. Rep. 6 (2016) 34503.
[46] D. Marangon, et al., In vivo silencing of miR-125a-3p promotes myelin repair in models of white matter demyelination, Glia 68 (10) (2020) 2001–2014.
[47] D. Marangon, M.P. Abbracchio, D. Lecca, Pathway-focused profiling of oligodendrocytes over-expressing miR-125a-3p reveals alteration of wnt and cell-to-cell signaling, Cell. Mol. Neurobiol. 41 (1) (2021) 105–114.
[48] X. Wang, et al., Ibuprofen enhances recovery from spinal cord injury by limiting tissue loss and stimulating axonal growth, J. Neurotrauma 26 (1) (2009) 81–95.
[49] J. Dill, et al., A molecular mechanism for ibuprofen-mediated RhoA inhibition in neurons, J. Neurosci. 30 (3) (2010) 963–972.
[50] B. Bodini, et al., Dynamic imaging of individual remyelination profiles in multiple sclerosis, Ann. Neurol. 79 (5) (2016) 726–738.
[51] M.S.Y. Yeung, et al., Dynamics of oligodendrocyte generation in multiple sclerosis, Nature 566 (7745) (2019) 538–542.
[52] M. Zawadzka, et al., CNS-resident glial progenitor/stem cells produce schwann cells as well as oligodendrocytes during repair of CNS demyelination, Cell Stem Cell 6 (6) (2010) 578–590.
[53] R.B. Tripathi, et al., NG2 glia generate new oligodendrocytes but few astrocytes in a murine experimental autoimmune encephalomyelitis model of demyelinating disease, J. Neurosci. 30 (48) (2010) 16383–16390.
[54] A.M. Falcão, et al., Disease-specific oligodendrocyte lineage cells arise in multiple sclerosis, Nat. Med. 24 (12) (2018) 1837–1844.
[55] S. Jäkel, et al., Altered human oligodendrocyte heterogeneity in multiple sclerosis, Nature 566 (7745) (2019) 543–547.
[56] E.P. Makhija, et al., Mechanical regulation of oligodendrocyte biology, Neurosci. Lett. 717 (2020), 134673.
[57] E.D. Carvalho, et al., A paradigm shift: bioengineering meets mechanobiology towards overcoming remyelination failure, Biomaterials 283 (2022), 121427.
[58] G. Ponath, C. Park, D. Pitt, The role of astrocytes in multiple sclerosis, Front. Immunol. 9 (2018) 217.
[59] D. Marangon, et al., Novel in vitro experimental approaches to study myelination and remyelination in the central nervous system, Front. Cell. Neurosci. 15 (2021), 748849.
[60] C.L. Howe, Coated glass and vicryl microfibers as artificial axons, Cells Tissues Organs 183 (4) (2006) 180–194.
[61] Y. Li, et al., Nanofibers support oligodendrocyte precursor cell growth and function as a neuron-free model for myelination study, Biomacromolecules 15 (1) (2014) 319–326.
[62] D. Liewald, et al., Distribution of axon diameters in cortical white matter: an electron-microscopic study on three human brains and a macaque, Biol. Cybern. 108 (5) (2014) 541–557.
[63] A. Saliani, et al., Axon and myelin morphology in animal and human spinal cord, Front. Neuroanat. 11 (2017) 129.
[64] D. Espinosa-Hoyos, et al., Engineered 3D-printed artificial axons, Sci. Rep. 8 (1) (2018) 478.
[65] A.N. Cho, et al., Aligned brain extracellular matrix promotes differentiation and myelination of human-induced pluripotent stem cell-derived oligodendrocytes, ACS Appl. Mater. Interfaces 11 (17) (2019) 15344–15353.
[66] S.J. Chun, et al., Integrin-linked kinase is required for laminin-2-induced oligodendrocyte cell spreading and CNS myelination, J. Cell Biol. 163 (2) (2003) 397–408.
[67] M.C. Weiger, et al., Spontaneous phosphoinositide 3-kinase signaling dynamics drive spreading and random migration of fibroblasts, J. Cell Sci. 122 (Pt 3) (2009) 313–323.
[68] K.W. Lee, et al., α-poly-L-lysine functions as an adipogenic inducer in 3T3-L1 preadipocytes, Amino Acids 53 (4) (2021) 587–596.
[69] M. Zeger, et al., Insulin-like growth factor type 1 receptor signaling in the cells of oligodendrocyte lineage is required for normal in vivo oligodendrocyte development and myelination, Glia 55 (4) (2007) 400–411.
[70] S. Ebner, M. Dunbar, R.D. McKinnon, Distinct roles for PI3K in proliferation and survival of oligodendrocyte progenitor cells, J. Neurosci. Res. 62 (3) (2000) 336–345.
[71] Y. Zhang, et al., An RNA-sequencing transcriptome and splicing database of glia, neurons, and vascular cells of the cerebral cortex, J. Neurosci. 34 (36) (2014) 11929–11947.
[72] P. Andjus, et al., Extracellular vesicles as innovative tool for diagnosis, regeneration and protection against neurological damage, Int. J. Mol. Sci. 21 (18) (2020).
[73] E. Pishavar, et al., Exosomes as neurological nanosized machines, ACS Nanoscience Au 2 (4) (2022) 284–296.
[74] I. Glezer, S. Rivest, Oncostatin M is a novel glucocorticoid-dependent neuroinflammatory factor that enhances oligodendrocyte precursor cell activity in demyelinated sites, Brain Behav. Immun. 24 (5) (2010) 695–704.
[75] L.L. Sarlième, A. Rodríguez-Peña, K. Langley, Expression of thyroid hormone receptor isoforms in the oligodendrocyte lineage, Neurochem. Res. 29 (5) (2004) 903–922.
[76] X. Zhao, et al., MicroRNA-mediated control of oligodendrocyte differentiation, Neuron 65 (5) (2010) 612–626.
[77] L. Ninio-Many, et al., microRNA-125a-3p reduces cell proliferation and migration by targeting Fyn, J. Cell Sci. 126 (Pt 13) (2013) 2867–2876.
[78] R. White, et al., Activation of oligodendroglial Fyn kinase enhances translation of mRNAs transported in hnRNP A2-dependent RNA granules, J. Cell Biol. 181 (4) (2008) 579–586.
[79] J.P. Michalski, R. Kothary, Oligodendrocytes in a nutshell, Front. Cell. Neurosci. 9 (2015) 340.
[80] X. Liang, N.A. Draghi, M.D. Resh, Signaling from integrins to Fyn to rho family GTPases regulates morphologic differentiation of oligodendrocytes, J. Neurosci. 24 (32) (2004) 7140–7149.
[81] B. García-Díaz, et al., Loss of lysophosphatidic acid receptor LPA1 alters oligodendrocyte differentiation and myelination in the mouse cerebral cortex, Brain Struct. Funct. 220 (6) (2015) 3701–3720.
[82] Y. Miyamoto, et al., Expression of kinase-deficient MEK2 ameliorates pelizaeus-merzbacher disease phenotypes in mice, Biochem. Biophys. Res. Commun. 531 (4) (2020) 445–451.
[83] A. Ishii, M. Furusho, R. Bansal, Sustained activation of ERK1/2 MAPK in oligodendrocytes and schwann cells enhances myelin growth and stimulates oligodendrocyte progenitor expansion, J. Neurosci. 33 (1) (2013) 175–186.
[84] S. Vejar, et al., Connexin and pannexin-based channels in oligodendrocytes: implications in brain health and disease, Front. Cell. Neurosci. 13 (2019) 3.
[85] M.C. Ortega, et al., Neuregulin-1/ErbB4 signaling controls the migration of oligodendrocyte precursor cells during development, Exp. Neurol. 235 (2) (2012) 610–620.
[86] C.M. Willis, et al., Astrocyte support for oligodendrocyte differentiation can be conveyed via extracellular vesicles but diminishes with age, Sci. Rep. 10 (1) (2020) 828.
[87] A.D. Chaudhuri, et al., TNFα and IL-1β modify the miRNA cargo of astrocyte shed extracellular vesicles to regulate neurotrophic signaling in neurons, Cell Death Dis. 9 (3) (2018) 363.
[88] A. Datta Chaudhuri, et al., Stimulus-dependent modifications in astrocyte-derived extracellular vesicle cargo regulate neuronal excitability, Glia 68 (1) (2020) 128–144.
[89] M.T. Haindl, et al., The formation of a glial scar does not prohibit remyelination in an animal model of multiple sclerosis, Glia 67 (3) (2019) 467–481.
[90] A. Rolls, R. Shechter, M. Schwartz, The bright side of the glial scar in CNS repair, Nat Rev Neurosci 10 (3) (2009) 235–241.
[91] M.L. Elkjaer, et al., Unique RNA signature of different lesion types in the brain white matter in progressive multiple sclerosis, Acta Neuropathol. Commun. 7 (1) (2019) 58.
[92] J. Orthmann-Murphy, et al., Remyelination alters the pattern of myelin in the cerebral cortex, elife (2020) 9.
[93] S. Chandler, et al., Matrix metalloproteinases degrade myelin basic protein, Neurosci. Lett. 201 (3) (1995) 223–226.

[94] K. Gijbels, R.E. Galardy, L. Steinman, Reversal of experimental autoimmune encephalomyelitis with a hydroxamate inhibitor of matrix metalloproteases, J. Clin. Invest. 94 (6) (1994) 2177–2182.
[95] L.W. Lau, et al., Chondroitin sulfate proteoglycans in demyelinated lesions impair remyelination, Ann. Neurol. 72 (3) (2012) 419–432.
[96] J.C. Pendleton, et al., Chondroitin sulfate proteoglycans inhibit oligodendrocyte myelination through PTPσ, Exp. Neurol. 247 (2013) 113–121.
[97] Z. Su, et al., Reactive astrocytes inhibit the survival and differentiation of oligodendrocyte precursor cells by secreted TNF-α, J. Neurotrauma 28 (6) (2011) 1089–1100.
[98] Y. Wang, et al., Astrocytes from the contused spinal cord inhibit oligodendrocyte differentiation of adult oligodendrocyte precursor cells by increasing the expression of bone morphogenetic proteins, J. Neurosci. 31 (16) (2011) 6053–6058.
[99] K. Sekiyama, et al., Ibuprofen ameliorates protein aggregation and astrocytic gliosis, but not cognitive dysfunction, in a transgenic mouse expressing dementia with Lewy bodies-linked P123H β-synuclein, Neurosci. Lett. 515 (1) (2012) 97–101.
[100] J.A. Wixey, et al., Ibuprofen treatment reduces the neuroinflammatory response and associated neuronal and white matter impairment in the growth restricted newborn, Front. Physiol. 10 (2019) 541.
[101] S.K. Mishra, M. Hidau, S. Rai, Memantine and ibuprofen pretreatment exerts anti-inflammatory effect against streptozotocin-induced astroglial inflammation via modulation of NMDA receptor-associated downstream calcium ion signaling, Inflammopharmacology 29 (1) (2021) 183–192.
[102] B. Xing, et al., RhoA-inhibiting NSAIDs promote axonal myelination after spinal cord injury, Exp. Neurol. 231 (2) (2011) 247–260.
[103] S. Sawaguchi, et al., Hypomyelinating leukodystrophy 7 (HLD7)-associated mutation of POLR3A is related to defective oligodendroglial cell differentiation, which is ameliorated by ibuprofen, Neurol. Int. 14 (1) (2022) 11–33.
[104] G.R. John, Investigation of astrocyte - oligodendrocyte interactions in human cultures, Methods Mol. Biol. 814 (2012) 401–414.
[105] Z. Liu, et al., Astrocytes induce proliferation of oligodendrocyte progenitor cells via connexin 47-mediated activation of the ERK/Id4 pathway, Cell Cycle 16 (7) (2017) 714–722.